Clim Dyn (2018) 50:1067–1090
DOI 10.1007/s00382-017-3661-6

Variability and trends of wet season temperature in the Sudano-Sahelian zone and relationships with precipitation

Boutheina Oueslati[1] · Pierre Camberlin[1] · Joël Zoungrana[2] · Pascal Roucou[1] · Saliou Diallo[1]

Received: 17 November 2016 / Accepted: 23 March 2017 / Published online: 5 April 2017

Abstract The relationships between precipitation and temperature in the central Sudano-Sahelian belt are investigated by analyzing 50 years (1959–2008) of observed temperature (Tx and Tn) and rainfall variations. At daily time-scale, both Tx and Tn show a marked decrease as a response to rainfall occurrence, with a strongest departure from normal 1 day after the rainfall event (−0.5 to −2.5 °C depending on the month). The cooling is slightly larger when heavy rainfall events (>5 mm) are considered. The temperature anomalies weaken after the rainfall event, but are still significant several days later. The physical mechanisms accounting for the temperature response to precipitation are analysed. The Tx drop is accounted for by reduced incoming solar radiation associated with increased cloud cover and increased surface evaporation following surface moistening. The effect of evaporation becomes dominant a few days after the rainfall event. The reduced daytime heat storage and the subsequent sensible heat flux result in a later negative Tn anomaly. The effect of rainfall variations on temperature is significant for long-term warming trends. The rainfall decrease experienced between 1959 and 2008 accounts for a rainy season Tx increase of 0.15 to 0.3 °C, out of a total Tx increase of 1.3 to 1.5 °C. These results have strong implications on the assessment of future temperature changes. The dampening or amplifying effects of precipitation are determined by the sign of future precipitation trends. Confidence on temperature changes under global warming partly depend on the robustness of precipitation projections.

Keywords Rainfall · Temperature · Climate change · Trends · Sahel · Burkina Faso

1 Introduction

Quantifying recent and future warming rates is an important issue in climatological research. While increases in greenhouse gases (GHG) concentrations are a key factor accounting for both global and regional warming trends, a number of other factors may either have an enhancing or dampening effect on these trends at local and regional scales. This includes the influence of several components of the water cycle such as the cooling effect of clouds at daytime and that of the evaporation of surface soil moisture, for instance. Whenever these components of the hydrologic cycle show long-term trends, this may affect temperature trends themselves. For instance, the "warming hole" (i.e., absence of warming trend) found over the east-central United States since the 1950s has been attributed to precipitation changes, cloud cover increases and shortwave cloud forcing due to aerosols (Pan et al. 2004; Portmann et al. 2009; Tang and Leng 2013; Yu et al. 2014). Over Eurasia, Tang and Leng (2012) found a summer temperature dependence on cloud cover at the high latitudes and in the midlatitude wet areas, and a dependence on precipitation in southern and central Asia. The damped warming trend observed from 1982 to 2009 in Western Siberia was associated with a cloud cover increase, while the strong warming in Europe was accompanied by a cloud cover decrease, suggesting that locally cloud cover (and precipitation over some regions) modulates summer temperature

✉ Boutheina Oueslati
oueslati@lsce.ipsl.fr

[1] Centre de Recherches de Climatologie/Biogéosciences, UMR 6282 CNRS, Univ. Bourgogne Franche-Comté, 21000 Dijon, France

[2] ASECNA, CP 806, Bissau, Guinea-Bissau

changes. Dong et al. (2016) noted that over Western Europe the rapid summer warming was explained by the combined effect of sea-surface temperature changes, GHG increases and reduced anthropogenic aerosols, but with important positive feedbacks from the drying of the land surface and the reduced cloudiness.

At global scale, there is a strong anti-correlation between precipitation and daytime maximum temperature from daily to interannual time-scales (Dai et al. 1999). However, the spatial and seasonal patterns of interannual temperature-precipitation relationships are complex (Trenberth and Shea 2005; Déry and Wood 2005; Adler et al. 2008; Berg et al. 2015). Although negative correlations tend to dominate tropical land areas, it is uneasy to fully understand the mechanisms behind the temperature-precipitation relationship, more so because some discrepancies exist between numerical models (Berg et al. 2015). The role of changes in the water cycle on temperature variations is also shown in climate projections. Recent studies have emphasized the role of soil moisture feedback in amplifying the projected mid-latitude warming over land (Seneviratne et al. 2013; Lorenz et al. 2016). Douville et al. (2016) found that this feedback explains up to half of the increase in the severity of the heat waves by the late twenty-first century. Berg et al. (2015) noted that in the regions showing on interannual time scales a strong temperature-precipitation anticorrelation, the projected long-term regional warming was partly modulated by the regional response of precipitation to global climate change. An analysis of the spatial patterns of observed warming rates (1979–2012) showed larger values in zones of lower vegetation indices (Zhou et al. 2015), suggesting negative feedbacks operate over wetter areas and ecosystems.

In West Africa, the sudano-sahelian belt has experienced huge decadal-scale variations in precipitation amounts since the 1950s, mainly in the form of a strong drying trend in the 1950–1990 period followed by a very partial recovery in the next two decades (Nicholson 2005; Lebel and Ali 2009). Similar variations were found in Burkina Faso, where the drought period climaxed in the mid-1980s (Lodoun et al. 2013; De Longueville et al. 2016). Meanwhile, rising temperatures were found over the region. Collins (2011) found a 0.12 to 0.19 °C/decade warming over tropical northern Africa (1979–2010). Note that the change was larger and more significant in the dry season (December–February) than in the wet season (June–August). Zhou et al. (2007) found that for the period 1950–2004, the largest world declines in diurnal temperature range (DTR) occurred over arid or semiarid regions, particularly the West African Sahel. DTR interannual variations are inversely related to those of Sahelian rainfall (and clouds at annual time-scale, their Table 1), although the DTR long-term trend cannot be accounted for by changes in rainfall and cloud cover. Ringard et al. (2016) analysed the seasonal temperature trends (Tx, Tn and extremes) over the Sahel (10°–20°N; 10°W–10°E), using the homogenized Berkeley Earth Surface Temperatures observation data set (Rohde et al. 2013). They found that since the mid-twentieth century the nocturnal/Tn warming was greater than the diurnal/Tx warming, although the opposite occurred over the post-1980s period. Moron et al. (2016) analyzed both the "Global Surface Summary of the Day" (GSOD version 7; Lott et al. 2008) and the "Global Historical Climate Network" (GHCN; Menne et al. 2012) datasets in Northern Tropical Africa from 1961 to 2014. They showed that annual mean Tx and Tn are increasing with linear trends equal to +0.20 °C/decade and +0.28 °C/decade, respectively. This significant warming is associated with more frequent warm temperatures over the 90th percentiles, as well as longer durations and higher occurrences of heat waves in both synoptic observations (Moron et al. 2016), NCEP/NCAR (Fontaine et al. 2013) and ERA-interim/ECMWF (Oueslati et al. 2017) reanalyses. Over Burkina Faso, De Longueville et al. (2016) found very significant trends in both cold extremes (negative trends) and warm extremes (positive trends) from 1950 to 2013.

Table 1 Linear temperature trends for Burkina Faso as a whole (average of nine stations), May–October, over the early and late parts of the study period. The p values of the F statistics are shown between brackets

	Tx (°C per decade)	Tn (°C per decade)
1959–1983	+0.49 (p = 0.995)	+0.54 (p > 0.999)
1984–2008	+0.28 (p = 0.860)	+0.57 (p > 0.999)

Several studies, in particular within the African Monsoon Multidisciplinary Analysis (AMMA) program, have documented the responses of the radiative balance and surface fluxes to convection in the Sudan and the Sahel. Taylor et al. (2005) noted that surface temperature in the 2000 rainy season, estimated from Meteosat data for the Sahel band, drops sharply after rainfall and increases gradually in the following days as the surface dries up. Schwendike et al. (2010), based on data collected from field campaigns in southern Burkina Faso, found that mesoscale convective systems (MCS) resulted in a surface temperature drop by up to 10 °C, and an increase in evapotranspiration by up to 2.5 $mm.d^{-1}$, which largely diminished within 2 to 3 days. Once the vegetation is well established, the amplitude of the response is weaker. Guichard et al. (2009), based on data collected in the Gourma region of Sahelian Mali, also noted the sharp drops in 2-m temperature accompanying rainfall events. As a result of thick cloud covers, they found occasional reductions of incoming solar radiation of large magnitude during the rainy season, these variations having a much greater control on surface incoming radiative flux

than those of downward longwave radiation. Further observations from Sahelian sites in Niger clearly show a strong decrease in sensible heat flux immediately after each rainfall event, and a parallel increase in latent heat flux (Guichard et al. 2012). These variations gradually vanish after a few days. In a wetter context, flux monitoring of the 2008 season at Nalahou (northern Benin, Sudanian climate) similarly shows strong day-to-day variations of net shortwave radiation, related to changes in cloud cover (Mamadou et al. 2014). These studies provided detailed accounts of seasonal and diurnal variations (and to some extent day-to-day variations) of the local energy balance during the monsoon season in the sudano-sahelian belt. However, the overall statistical relationship between temperature variations and rainfall at daily time-scale and over a large area has not been studied, and the contribution of this relationship to interannual variability and long-term climate trends is also unknown.

In this study, we document the lead-lag relationships between these two parameters (precipitation and temperature) at the scale of Burkina Faso, in the central part of the sudano-sahelian belt, and their possible contribution to explain part of the long-term warming trends. Both daily and annual time-scales are considered. The aim is first to assess how daily temperature (maximum and minimum) responds to a rainfall event occurring either the same day or on previous days. This response is then extracted from the daily temperature variations, and the residual temperature signal is analysed for long-term trends. Daily maximum (Tx) and minimum (Tn) temperatures are considered separately since their relationship to cloud cover and precipitation are likely to be different, as shown for eastern Africa (Camberlin 2016). Physical mechanisms accounting for the temperature response to precipitation variations are also discussed by considering reanalysis and remote sensed data.

Section 2 describes the data sets and the methodology. The daily temperature variations associated with rainfall occurrence and their interpretation are presented in Sect. 3. The long-term temperature trends and the possible contribution of rainfall variations to these trends are finally investigated in Sect. 4.

2 Data and methods

Most of Burkina Faso lies in the Sudanian zone of West Africa, characterized by a single, relatively long rainy season starting in April–May and ending in October, and a mean annual rainfall in the range of 600–1100 mm (Fig. 1). The northern part of the country lies in the drier Sahelian zone, and has a shorter rainy season (June–September) and lower annual rainfall (400–600 mm). August is the wettest month at all locations. Mean monthly temperature during the rainy season is high (25–33 °C), with warmest conditions shortly before and in the early part of the rainy season (April–May), a moderate decrease in the middle of the rainy season (August), followed by a small increase.

Daily precipitation data for nine stations were obtained from Direction Générale de la Météorologie du Burkina Faso (DGMB). Over the period 1959–2008, the data are almost complete (from 0.01 to 0.61% of missing values depending on the station). A comparison was made with the corresponding data from the global summary of the day (GSOD) dataset archived by NOAA (http://www1.ncdc.noaa.gov/pub/data/gsod). Evidence was found of small number of discrepancies, including a 1-day lag in some instances, as well as a few unreported rainfall events and incorrect truncations in GSOD. Given that data from the national meteorological service was first hand, priority was given to it. The stations are located between 10°N and 14°N (Fig. 1), with a strong meridional gradient in mean annual precipitation between the southernmost station, Gaoua (1058 mm and 74 rainy days), and the northernmost station, Dori (481 mm and 37 rainy days) (Fig. 1).

Daily maximum (Tx) and minimum (Tn) air temperatures (at 2 meters) are extracted from the global historical climate network daily (GHCND) data set (Menne et al. 2012). They have been supplemented by GSOD data. To match the rainfall data, the same nine stations were retained, each one having at least 6200 available daily temperature records (equivalent to 17 full years) over the period 1959–2008. In the final analysis dedicated to the assessment of the regional temperature trend over the full 50-year period, only six stations were retained, due to too many missing temperature data (>20%) at Ouahigouya, Dédougou and Po. Daily temperature data from DMGB could only be obtained for 1 year (2008). They were used for quality control of the GSOD data. The comparison revealed that most of the time the two data sets were in very good agreement at all the nine stations. Over 2422 daily observations, the correlation coefficients between DMGB and GSOD data at zero lag are 0.994 and 0.987 for Tx and Tn respectively. The root-mean square error is 0.4 °C for Tx and 0.63° for Tn, for which there exists a small positive bias in GSOD.

In principle, daily observations in both the GHCND and GSOD data sets cover the 24-h period between 0000 and 2359 GMT (local time in Burkina Faso is the same as GMT). However, 24-h records in GSOD may include a portion of the previous day (https://data.noaa.gov/dataset/global-surface-summary-of-the-day-gsod). Some discrepancies in the period covered by the 24-h record may also be found in the GHCND data, although the problem was mainly detected for some US stations (Menne et al. 2012). According to WMO standards, and as a rule in DGMB

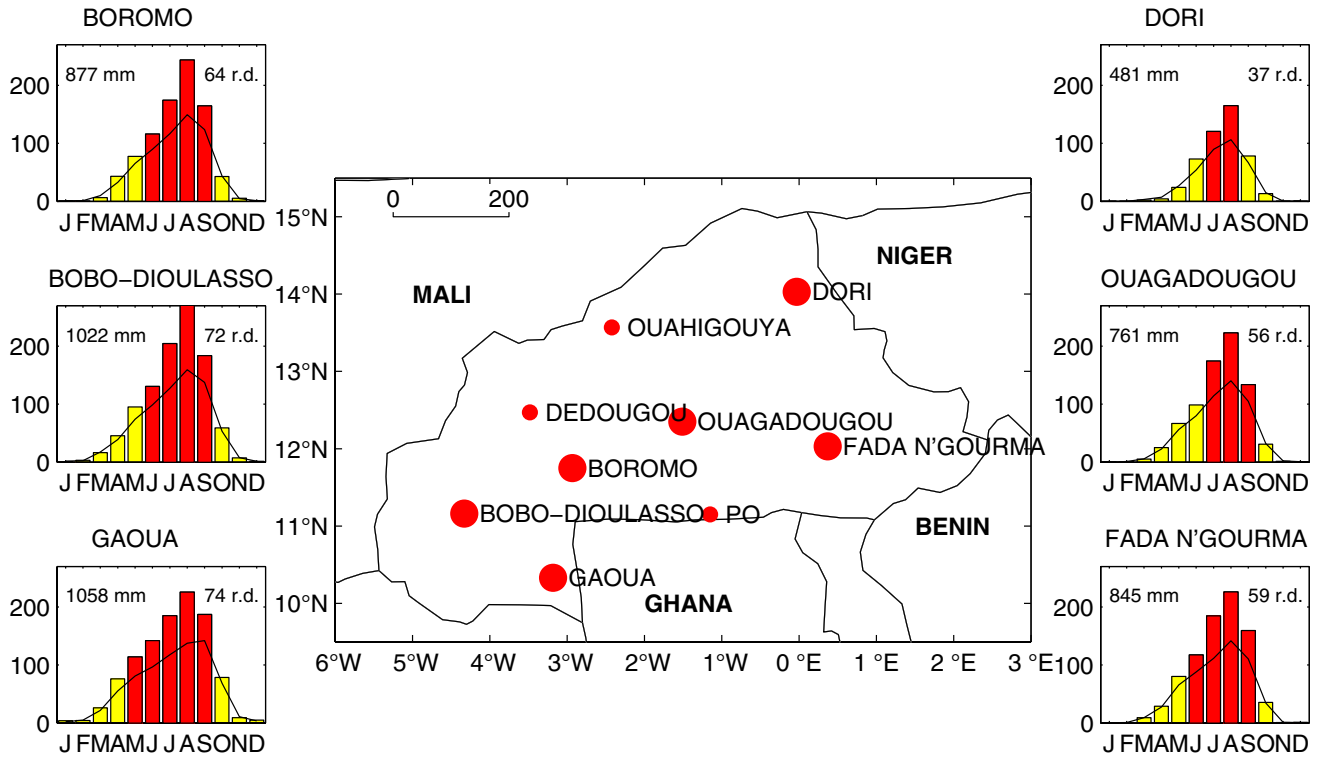

Fig. 1 Stations locations and mean rainfall regimes (1959–2008). *Large dots* indicate the six stations with the most complete temperature series and retained for the trend analysis. *Bars denote* mean monthly rainfall (mm, with months receiving over 100 mm in *red*); *black lines* are the mean monthly number of rain days (x10). The mean annual rainfall amounts and mean annual number of rain days are also provided

records, 24-h precipitation summaries should be recorded from 0601 to 0600 UTC the following day (WMO 2009). Since most precipitation is likely to fall in the 0600 to 2400 time span of the first day (especially in tropical land areas where an afternoon peak is common), the rainfall record should appropriately be allocated to the first day, which is not done in GSOD data. A comparison between precipitation from the DGMB national meteorological service and GSOD actually revealed that most of the time GSOD data were lagging by 1 day. While the problem of time stamping for precipitation is checked by giving priority to DGMB data, we cannot exclude that some of the temperature data were not affected. Although this issue may result in a small uncertainty in the exact timing of the response of temperature to rainfall events, it should not be seen as a major shortcoming since the extraction of the rainfall signal in the temperature time-series will consider several time lags.

Linear trends were analyzed using least mean squares regressions. For a comparison with seasonal trends over the Sudano-Sahelian belt as a whole, additional data were used. Monthly precipitation, Tx and Tn data from the Climatic Research Unit (CRU) 0.5° data base (Harris et al. 2014) were averaged over the region 15°W–20°E, 10–15°N, corresponding to the central part of the Sudano-Sahelian belt, and the period from May to October, which is the wet season in most of the region.

Relationships between daily temperature variations and precipitation were investigated by means of composite analyses, linear correlation and regression analyses, as in Camberlin (2016). Daily temperature anomalies were first obtained by removing from the raw data at each station a smoothed seasonal cycle (50-year daily average smoothed on 21-day running windows), and removing the long-term linear trend computed separately for each month. Then lead-lag composites of daily temperature anomalies for all days recording rainfall (at least 1 mm) were computed. Other composites were also computed using a higher rainfall threshold to test whether the temperature anomaly was dependent on the amount, and by considering different sequences of dry and wet days to test the effect of persistent rainfall or absence of rainfall. The corresponding temperature anomalies were tested for statistical significance using Student's t test. The analysis is first carried out at the station scale, then a composite index is computed for Burkina Faso as a whole (see below).

Given the fact the relationships between temperature and precipitation is sometimes found at different lags, a multiple linear model was designed at each station with

temperature on day d0 (T_0) as the dependent variable, and both precipitation occurrence (O) and amount (A) on days d-4 to d0 as predictors (Eq. 1):

$$T_0 = \sum_{i=-4}^{0} a_i.O_i + \sum_{j=-4}^{0} b_j.A_j + c \quad (1)$$

Predictors to be retained in the models were selected using a stepwise procedure. Note that of course occurrence and amount are strongly interrelated, but attempts to use only one of these variables gave coefficients of determination lower than when considering both variables as potential predictors. This will be discussed later. The inclusion of rainfall predictors for up to 4 days before the target day is justified in the composite analyses below. To account for seasonality, separate models are defined for each month of the rainy season.

Predicted daily temperature variations from these models are deducted from the raw data to obtain residual temperatures, i.e. with the effect of precipitation removed. These residuals are averaged at monthly and seasonal time-scales, then analyzed for linear trends over the period 1959–2008. This enabled to assess how much warming trend is left after extracting the temperature variations associated with those of rainfall.

The contribution of rainfall variations to those of temperature was also asserted at seasonal time-scale using simple linear regression. Raw seasonal temperature variations were regressed against seasonal rainfall amounts, and the temperature residuals analyzed for linear trends. These trends were compared with the long-term warming trends computed from the raw temperature data, and those obtained with above method to extract rainfall effect from daily temperature.

To further diagnose the thermodynamics associated with the rainfall events, data documenting the heat fluxes were extracted from the ERA-INTERIM reanalyses, produced by the ECMWF (Dee et al. 2011). They cover the 30-year period 1979–2008 at daily time-scale and include precipitation, 2-m maximum temperature (taken over the time period 1200 to 2400 GMT) and minimum temperature (taken from 0000 to 0600), daily sensible surface heat flux (SH), latent surface heat flux (LH) as well as daily surface net shortwave (SWR) and longwave radiation (LWR).. Note that the time span over which daily precipitation is accumulated (0000 to 2400) differs from the observation (0600 to 0600) which may slightly affect the comparison between the two data sets. This issue is further discussed below. In order to assess the quality of ERA-INTERIM in representing surface radiative fluxes, a comparison with the clouds and the earth's radiant energy system synoptic (CERES-SYN1deg) daily satellite product (Rutan et al. 2015) available from the period 2001–2008 is carried out. It includes both all-sky and clear-sky surface SWR and LWR. Shortwave (SWCRE) and longwave (LWCRE) cloud radiative effects are computed as the difference between all-sky and clear-sky surface net SWR and LWR.

An area-averaged index was defined, to identify regional-scale precipitation events and examine their relationship with temperature in the reanalysis fields. This was necessary since reanalysis data cannot be used to assess local-scale climate variations. This index is computed as the daily percentage of stations (out of nine stations, for the observation) and the daily percentage of grid-points within the 5°W–2°E, 10–15°N region (for ERA-INTERIM) which recorded rainfall of at least 1 mm. Days when the index is above 50 and 80% in GHCND and ERA-Interim, respectively, were retained for the composite analysis. Given that rainfall events in ERA-INTERIM tend to be more widespread than in the observation, different thresholds are necessary to obtain a sample of similar size to that used in the observation. Like for the analysis carried out at station scale, lead-lag daily mean anomalies were computed for each day from 4 days before to 7 days after the rainfall event.

3 Daily temperature variations associated with rainfall

3.1 Temperature composites

Composites of local daily temperature anomalies (Tx and Tn) associated with rain days (d0) are computed at each station and for each month. The composites extend from 4 days before to 7 days after d0. The results for the month of September, a typical month of the rainy season, and four sample stations are shown in Fig. 2. Rain days are defined as days with at least 1 mm (bold lines) or at least 15 mm (thin lines). The 15 mm threshold was chosen to single out relatively heavy rainfall events, with a third of the rain days exceeding this threshold during the May–October period for the nine stations combined. All stations show a fairly similar pattern, although the anomalies are larger at the drier (northernmost) stations. Rainfall events are characterized by a significant ($P = 0.99$) drop in both Tx and Tn, which is initiated at d0, at least for Tx, but is greatest at d+1. The temperature decrease on d+1 at Dori (northern Burkina Faso) is −1.3 to −1.5 °C, with little difference between Tx and Tn. Later on temperature rises up, but Tx still shows significant negative anomalies on d+2 and sometimes in the following days. On the other hand the Tn decrease is short-lived. Considering only heavy rainfall events (≥15 mm) results in stronger negative anomalies on d+1 and frequently in the following days as well, especially for Tx at the driest stations. This indicates that not

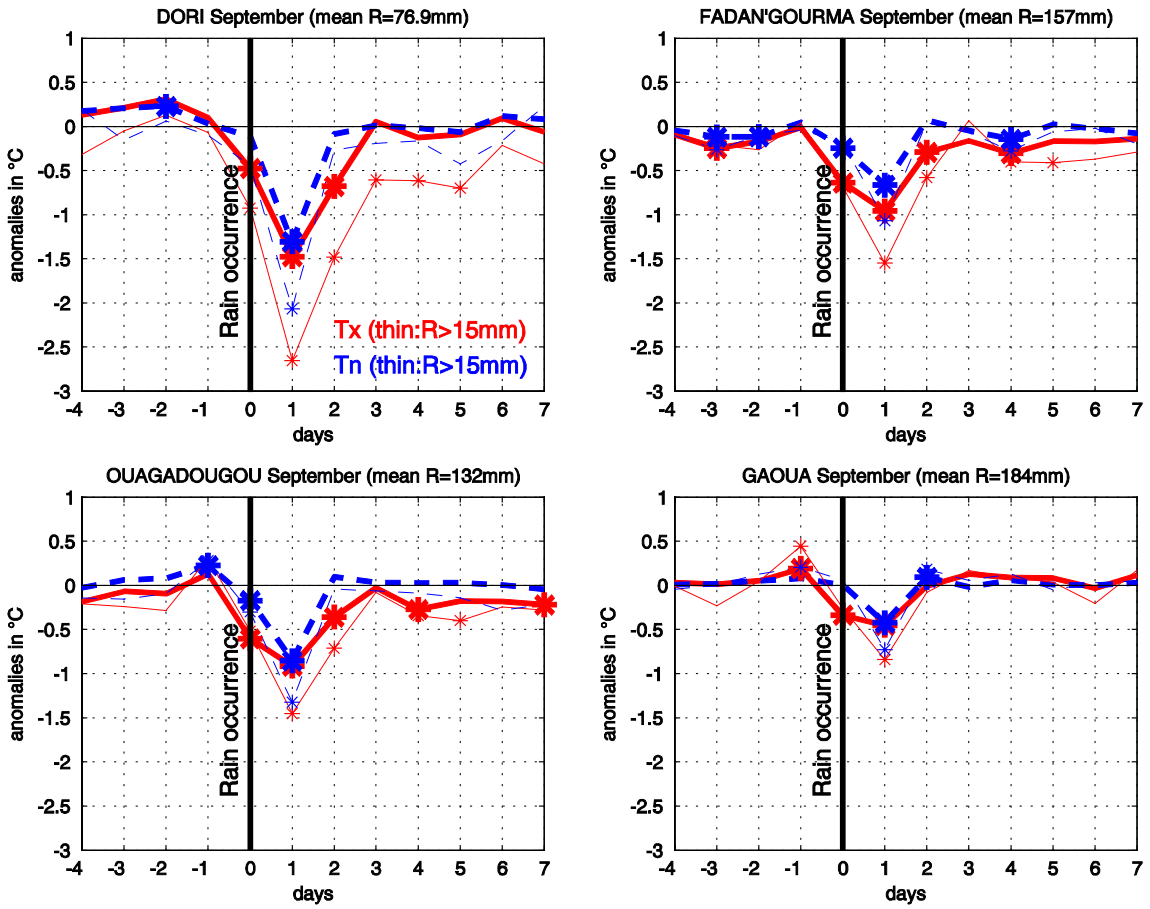

Fig. 2 Composite September temperature anomalies from 4 days before to 7 days after a rain-day (day 0), at sample four stations in Burkina Faso. Rain-days are defined as receiving at least 1 mm (*thick lines*) or 15 mm (*thin lines*). *Stars* show significant anomalies (P = 0.95) according to a Student's *t* test. The September mean rainfall amount is shown above each panel

only rainfall occurrence but also its intensity has an effect on surface temperature.

Since the composites are fairly similar throughout Burkina Faso, a regional composite combining the nine stations is constructed by selecting all days where over 50% of the stations across the country were recording rainfall (1 and 15 mm thresholds). For the May–October period, this represents 20% of the total number of days (for the 1 mm threshold). The temperature anomalies averaged over the nine stations and the days selected for these composites are plotted for each month of the May–October period (Fig. 3). On the whole, little differences are found between the 6 months although the anomalies are stronger in the driest months (especially May and October) and smaller in the peak rainfall month of August. All months show a highly significant (P = 0.99) temperature decrease associated with the rainfall events, which is most pronounced on the day following the rain (d+1). Both Tx and Tn are affected, and in the first part of the rainy season (May–July) the Tn decrease is as large as that of Tx, reaching −2.3 °C in May. Later in the season, the Tx decrease becomes stronger (e.g., −2 °C in October as against −0.8 °C for Tn). For Tx, the decrease is already apparent on d0, although it is much smaller than on d+1. As noted earlier for September, Tx anomalies remain negative and often significant for several days after the rainfall event. These anomalies are slightly larger when the sample is based on heavier rainfall days only (over 5 mm, thin lines). Note that in July–August the day preceding the rainfall event (d−1) is slightly warmer than normal. This can be related to the results of Taylor et al. (2011) who showed that convection triggering is enhanced by mesoscale heterogeneity of surface soil moisture with convection tending to develop over dry warm areas.

Given that the above composites are based on any rain day, with no consideration whether the preceding and following days are themselves dry or wet, additional analyses have been carried out by defining different samples of consecutive wet and dry days. Temperature anomalies for totally dry spells are compared to spells starting with a wet day (1 mm threshold, Fig. 4). When comparing a sequence of a wet day followed by a dry day ("10") to

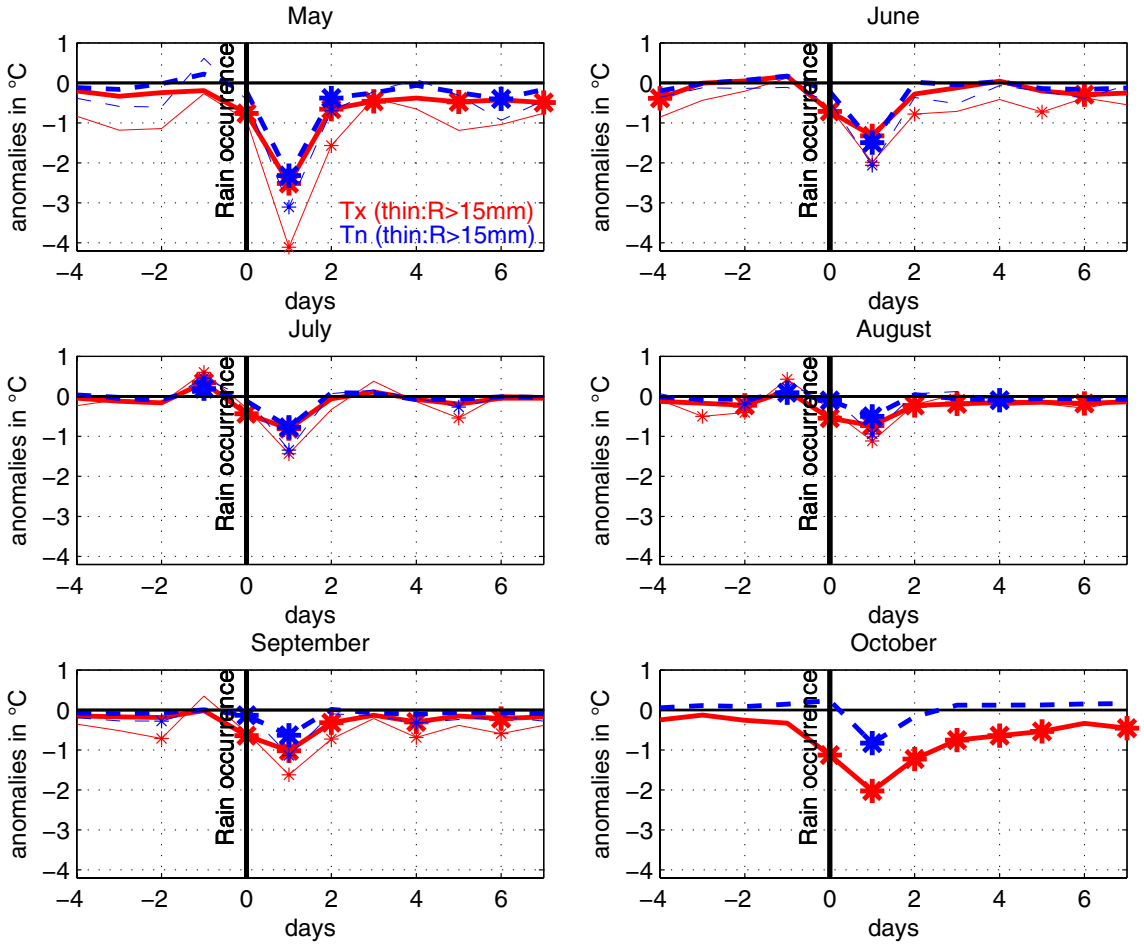

Fig. 3 Composite temperature anomalies over Burkina Faso as a whole (average of nine stations) from 4 days before to 7 days after a rain-day (day 0) in the observed data, from May to October. Rain days defining the composite sample are days where over 50% of the stations received at least 1 mm (*thick lines*) or 15 mm (*thin lines*). *Stars* show significant anomalies (P = 0.99) according to a Student's *t* test

a sequence of two dry days ("00"), large and significant (stars, t-test, P = 0.99) temperature differences are found on the second day between the two samples. This applies to both Tx and Tn in any month from May to October (Fig. 4, second row), but the difference is particularly large for Tx at the beginning and end of the rainy season (temperatures 1.5 to 2.5 °C lower following a wet day) and at the beginning of the rainy season (2–3 °C) for Tn. It is also shown that these differences are much larger than when simply comparing the temperature of wet days to that of dry days (Fig. 4, first row). It is noteworthy that at the end of 3 days sequences there is still a difference of 0.8 to 1.3 °C in Tx (significant at most stations, Fig. 4, third row), suggesting that the cooling effect of a wet day on Tx is still felt 2 days after the rain occurred. The cooling effect is found on Tn as well, but only at the beginning of the rainy season. At the end of a sequence of 4 days, there is still a small difference (0.2 to 0.8 °C) in Tx, which is significant at most stations, especially in the early part of the monsoon season (Fig. 4, fourth row). The effect on Tn is weaker and restricted to May and June. Significance is lost at the end of 5-day sequences at most stations, although a 0.5 °C average difference is still found for Tx. Note that using more complex sequences (green lines, middle Tx panels) further indicate that several consecutive wet days (e.g., "1100" sequences) result in cooler conditions, even 2 days after the end of the rains, than isolated wet days ("0100" sequences), but in the early stage of the season only. When a higher precipitation threshold is retained (e.g., 15 mm instead of 1 mm, not shown), similar patterns are obtained except that the temperature differences between wet and dry sequences are larger, and the effect on Tn much less durable than that on Tx. On the whole, these results suggest that the "memory" of a rainfall event in the temperature anomalies lasts for about 3–4 days.

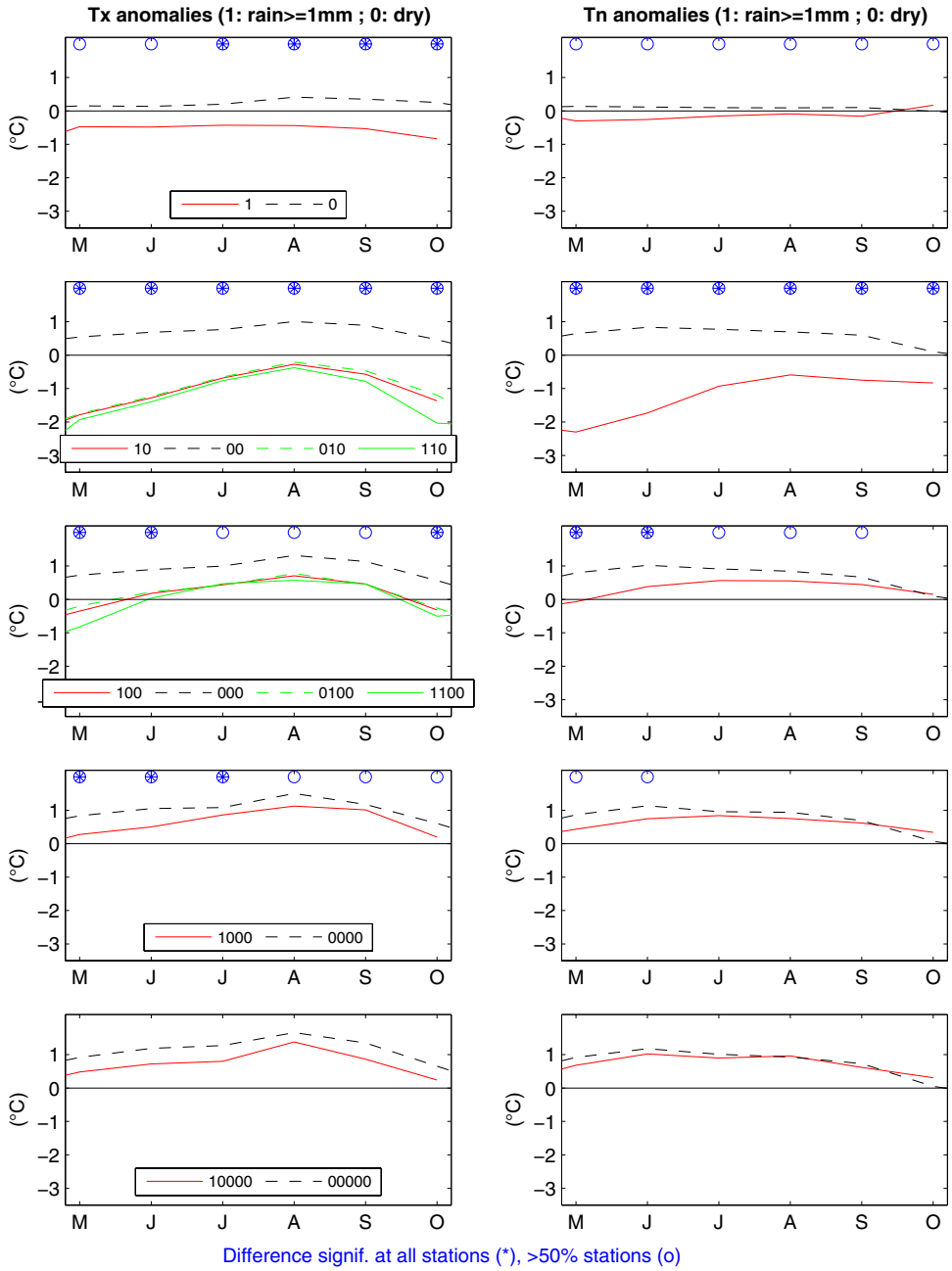

Fig. 4 Composite temperature anomalies (average of nine stations across Burkina Faso) for the last day of different sequences of wet and dry days. "1" stands for a rain day (1 mm or more) and "0" for a dry day. For instance, composite "1000" shows the temperature anomalies found on the last day of a sequence of one wet day followed by three dry days, and composite "0000" is the same but for a sequence of four dry days. *Blue circles* at the top of each subplot denote months for which the difference between temperature anomalies from the two main samples (*solid red* and *black* dashed *lines*) is significant (t test, P = 0.99) for over 50% of the stations (*stars* significant for all stations)

These results indicate a robust (in space and time) response of surface temperature to rainfall. The dominant lag between rainfall occurrence and temperature suggests that temperature responds to rainfall (or atmospheric variables related to rainfall), and not the reverse. Several candidates could explain the cooling found shortly after the rainfall event, including increased cloud cover, evaporation of precipitated water, or horizontal advection of cooler air. Reanalysis data are used, together with published material based on field campaigns, to discuss the mechanisms involved in the temperature variations.

3.2 Surface fluxes

This section documents day-to-day changes in several atmospheric variables, based on ERA-INTERIM reanalysis data for SH, LH, SWR and LWR and on CERES-SYN-1deg daily satellite product for SWR, LWR, SWCRE and LWCRE.

The use of reanalysis data to document surface fluxes is contingent upon the ability of ERA-INTERIM to reproduce the daily temperature-rainfall relationships depicted above. A first step is therefore to analyse these relationships

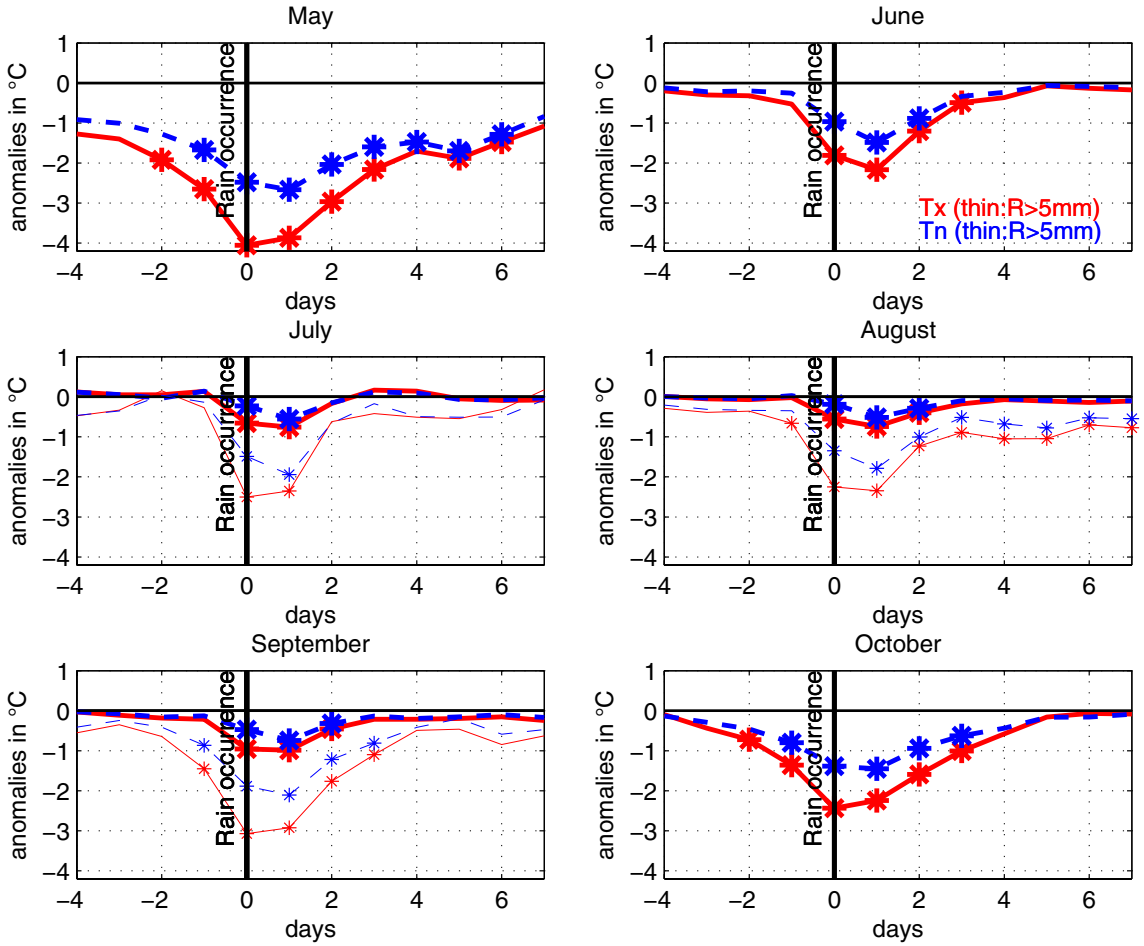

Fig. 5 Composite temperature anomalies over Burkina Faso as a whole (ERA-INTERIM reanalyses, average of all grid-points, period 1983–2008) from 4 days before to 7 days after a rain-day (day 0) in the reanalysis, from May to October. Tx is shown in *red* and *solid lines* and Tn in *blue* and *dashed lines*. Rain-days defining the composite sample are days where over 80% of the grid-points received at least 1 mm (*thick lines*) or 5 mm (*thin lines*). *Stars* show significant anomalies (P = 0.99) according to a Student's *t* test. There are not enough days in the samples at the 5 mm threshold in May, June and October for the composite anomaly to be computed. Tx is taken from the 0000 to 2400 interval, and Tn from the 0000 to 1200 interval

in ERA-INTERIM (Fig. 5). The same lead-lag temperature composites as for observed rainfall are computed, except that the retained spatial extension of the rainfall event is different between the two datasets (i.e. 80% of the grid-points for ERA-INTERIM and 50% for raingauge data), as explained earlier, and the threshold to discriminate the 33% heaviest rainfall events is lower (5 mm as against 15 mm). Rainfall events are accompanied and followed by a significant cooling (P = 0.99) in all months, and in both Tx and Tn, as in the observed data. The temperature decrease occurs generally slightly earlier than in the observation. While the largest anomalies are generally found on d+1, on d0 the anomalies are almost as large, or sometimes larger for Tx. This results from two facts : (1) the spatial smoothing inherent to ERA-INTERIM reanalyses, and (2) biases in the rainfall diurnal in cycle rainfall, since ERA-INTERIM, as many other global and regional climate models in the inland tropics, shows a strong maximum around noon (Betts et al. 2009; Nikulin et al. 2012), whereas in the observation rainfall peaks between 1500 and 2100 local time over West Africa, or later in the night where the influence of travelling systems is dominant (Roca et al. 2010; Nikulin et al. 2012). This unrealistic diurnal cycle results in temperature (especially Tx) being impacted earlier by precipitation occurrence than in the observation, where the maximum cooling is clearly on d+1. As in the observation, the temperature anomalies are larger in the drier months (e.g., May, June, October). The magnitude of the rainfall event also plays a role, actually more so than in the observation. For instance, August Tx anomalies for rainfall events above 1 mm are at −0.8 °C on d+1, but reach −2.3 °C for rainfall events above 5 mm. There is also some persistence of the negative anomalies beyond d+1, again with a larger magnitude than in the observation. For

instance, the cooling is still significant 7 days beyond the heavy (>5 mm) rainfall events in August, 3 days beyond in September. This could be associated with the so-called drizzle bias (e.g. Sun et al. 2006). Indeed, climate models tend to simulate higher frequency of low precipitation events resulting in an overestimated persistence of rainfall and temperature cooling (Fig. 5).

On the whole, the composite pattern remains reasonably similar to that found in the observations. This suggests that ERA-INTERIM can now be used to document surface radiative and turbulent fluxes possibly accounting for the cooling.

3.2.1 *Surface radiative fluxes*

Composites of daily SWR and LWR anomalies associated with rain days (d0) are computed for each month over Burkina Faso, for both ERA-INTERIM (Fig. 6) and CERES (Fig. 7) data. The radiative fluxes anomalies obtained from CERES are computed relative to rainfall events in GHCND. With the exception of the early part of the rainy season (especially May), the composite pattern of ERA-INTERIM is reasonably similar to that found in the observations. Rainfall events are accompanied and followed by a significant reduction in SWR in all months, resulting in Tx cooling. As in the observation, the radiative fluxes anomalies are larger in the driest months (e.g., May, June, October). The magnitude of the rainfall event in ERA-INTERIM plays a significant role, actually more so than in the observation, in consistency with temperature anomalies composites (Fig. 5). For instance, August SWR anomalies for rainfall events above 1 mm are at -10 Wm^{-2} on d0, but reach −40 W m^{-2} on the same day for rainfall events above 5 mm. In the reanalysis, there is also some persistence of the negative SWR anomalies beyond d+1. For instance, the SWR reduction is still significant

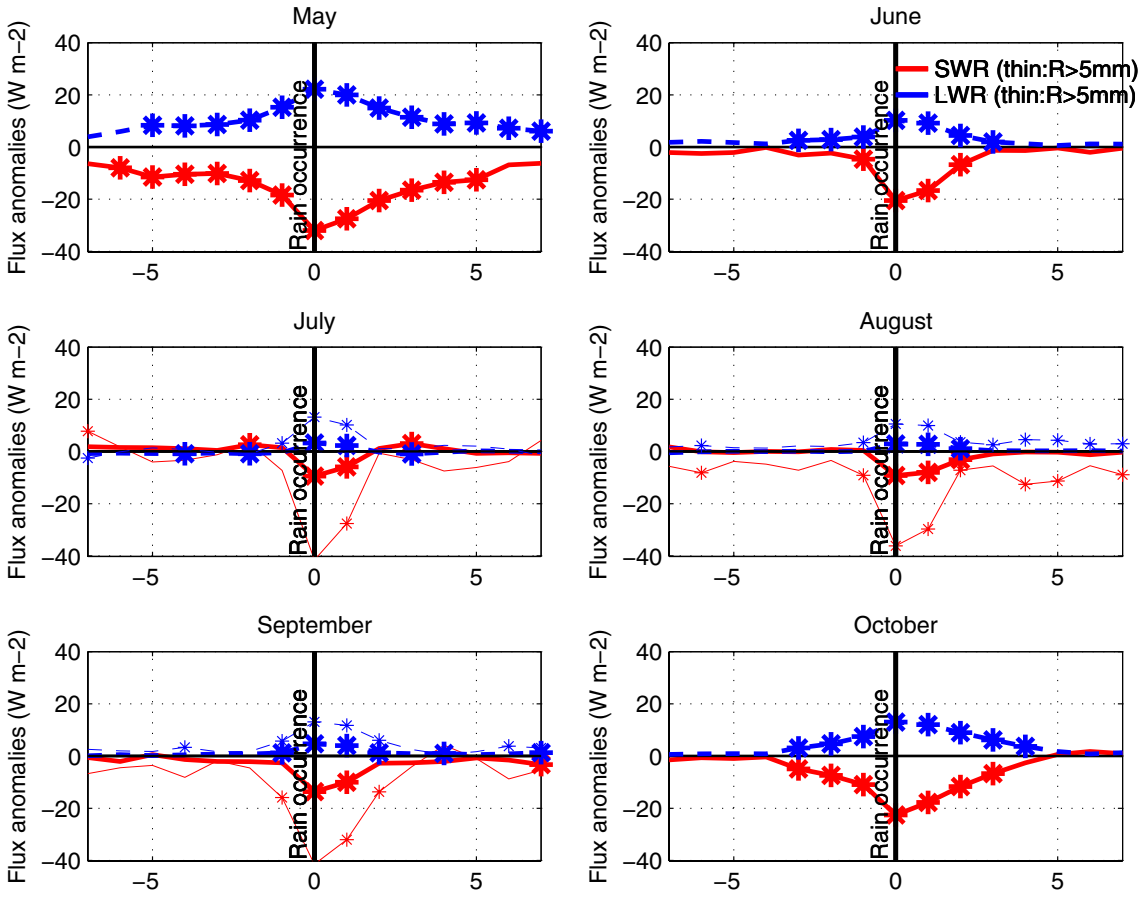

Fig. 6 Composite surface anomalies of shortwave radiation (*SWR*) and net longwave radiation (*LWR*) over Burkina Faso as a whole (ERA-INTERIM reanalyses, average of all grid-points, period 1983–2008) from 4 days before to 7 days after a rain-day (day 0) in the reanalysis, from May to October. SWR is shown in *red* and *solid lines* and LWR in *blue* and *dashed lines*. Rain-days defining the composite sample are days where over 80% of the grid-points received at least 1 mm (*thick lines*) or 5 mm (*thin lines*). Radiative fluxes are counted positive downwards so that negative (positive) anomalies of SWR (LWR) represent a radiative cooling (heating) of the surface. *Stars* show significant anomalies (P = 0.99) according to a Student's *t* test

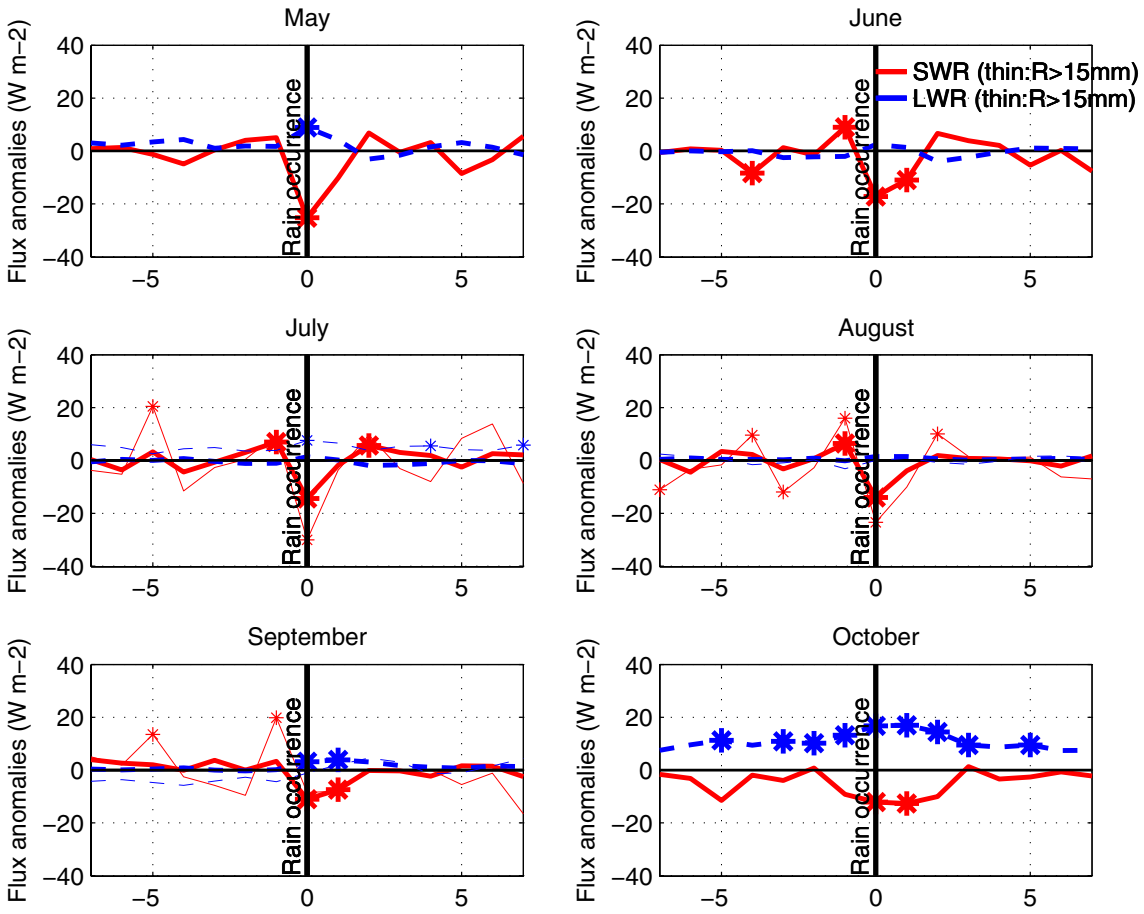

Fig. 7 Composite surface net SWR and LWR anomalies over Burkina Faso as a whole (CERES-SYN1deg data, average of all gridpoints, period 2001–2008) from 4 days before to 7 days after a rain-day (day 0) in observed data, from May to October. SWR is shown in *red* and *solid lines* and LWR in *blue* and *dashed lines*. Rain-days defining the composite sample are days in GHCND where over 50% of the stations received at least 1 mm (*thick lines*) or 15 mm (*thin* lines). Radiative fluxes are counted positive downwards so that negative (positive) anomalies of SWR (LWR) represent a radiative cooling (heating) of the surface. *Stars* show significant anomalies (P = 0.99) according to a Student's *t* test

7 days beyond the heavy (>5 mm) rainfall events in August, 3 days beyond in September, but this could be an artefact since there is virtually no signal in the satellite product. In the observation, the reduced SWR is limited to d0 and d+1. The reduction in the incoming SWR during the rainfall event is explained by an increase in SWCRE (Fig. 8) associated with an increased cloud cover and optical depth. LWR does not explain the temperature cooling. Indeed, positive anomalies are obtained during rainfall events, that are larger in the driest months (May and October), indicating that more infrared radiation is radiated back to the earth's surface, contributing in temperature warming. The anomalous downward LWR is not explained by the cloud greenhouse effect (Fig. 8) but is mainly associated with water vapor anomalies that are larger in the driest months, as highlighted in previous studies (e.g. Guichard et al. (2009)).

3.2.2 *Surface turbulent fluxes*

In this section, we explore the role of surface turbulent fluxes in temperature cooling using ERA-INTERIM data. It is important to be careful when using reanalyses because land surface states and fluxes are not assimilated and are based on the forecast model that is subject to errors and uncertainties. Because of the absence of flux towers in this region, the use of ERA-INTERIM is necessary to document the impact of surface turbulent fluxes, by focusing on the sensitivity of temperature to these fluxes. This is done using the Evaporative Fraction (EF) defined as the ratio of LH to the sum of LH and SH to document the partitioning of the available energy at the land surface into latent and sensible heat flux. Composites of EF mean and anomalies associated with rain days (d0) are computed as above, using ERA-INTERIM data (Fig. 9). Rainfall events are

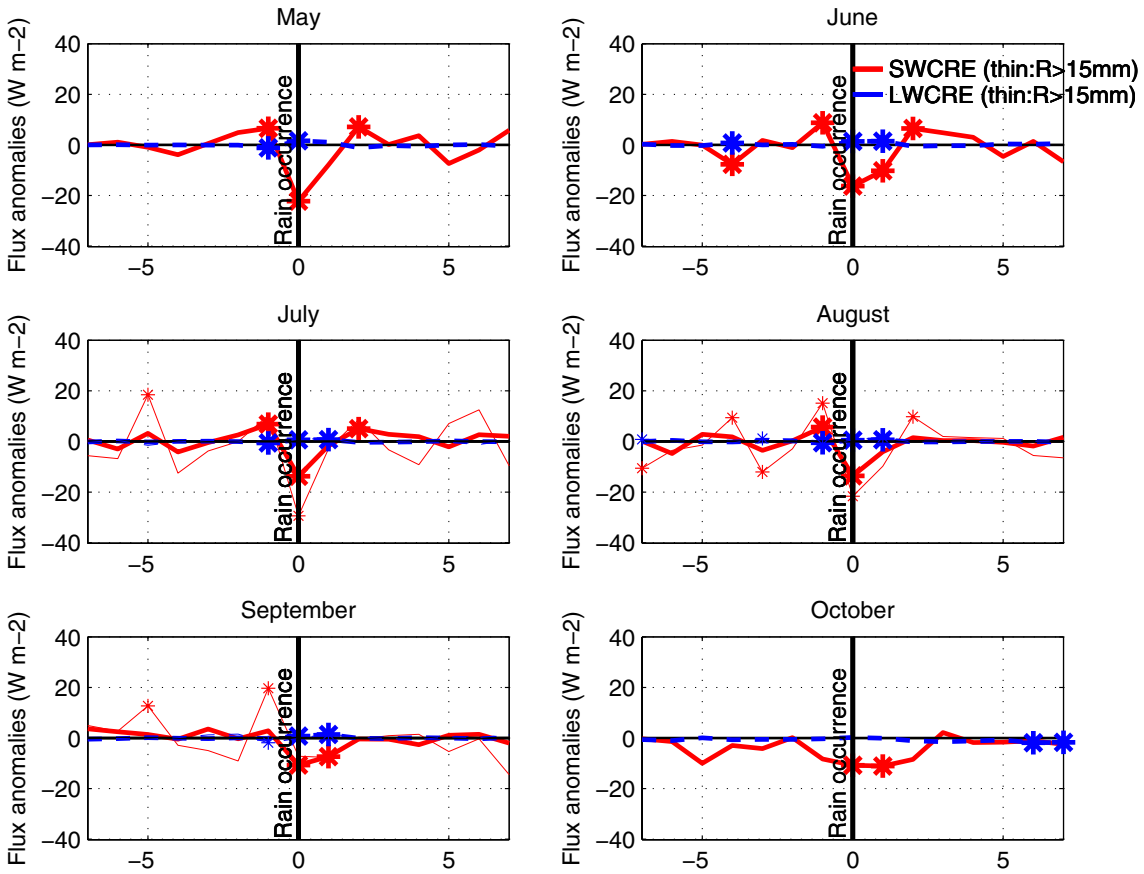

Fig. 8 Composite surface anomalies of shortwave (SWCRE) and longwave (LWCRE) cloud radiative effects over Burkina Faso as a whole (CERES-SYN1deg data, average of all grid-points, period 2001–2008) from 4 days before to 7 days after a rain-day (day 0), from May to October. SWCRE and LWCRE effects are computed as the difference between all-sky and clear-sky surface net SWR and LWR. SWCRE is shown in *red* and *solid lines* and LWCRE in *blue* and *dashed lines*. Rain-days defining the composite sample are days in GHCND where over 50% of the stations received at least 1 mm (*thick lines*) or 15 mm (*thin lines*). Negative anomalies of SWCRE correspond to a larger cooling effect of clouds at the surface. *Stars* show significant anomalies (P = 0.99) according to a Student's *t* test

accompanied and followed by a significant increase in EF in all months. EF is stronger for heavy rainfall events in the wettest months (July, August and September) and persists a long time (4–7 days) after rainfall occurrence. The heat flux due to surface evaporation is greater than the sensible heat flux during rainfall events and contributes significantly to the persistent temperature cooling (Fig. 5). This is explained by the larger amount of water available for evaporation and the persistence in time of soil moisture. This result suggests that the soil moisture-temperature coupling is important in the central part of the sudano-sahelian belt in consistency with other studies (e.g. Fischer et al. 2007a, b). After rain occurrence, EF decreases gradually following the increase in sensible heat flux and the drying of the surface. These results are consistent with Lohou et al. (2014) who examined the surface response to rain events using flux towers in Hombori (Mali), Niamey (Niger) and Djougou (Benin). They showed that the immediate surface response to rainfall event is an increase in EF that mainly depends on the soil moisture content. Several days after the rain, EF decreases following soil moisture depletion and vegetation drying. Land surface models describe relatively well the immediate response. However, the simulated decrease of EF is slower and weaker than observed.

Composites of daily SH and LH anomalies associated with rain days are shown in Fig. 10. In the wettest months, LH anomalies are close to zero before d0 and become larger after d+2, for heavy rainfall events only (Fig. 10). This is explained by the larger amount of soil moisture and the gradual increase of net shortwave radiation 2 days after precipitation occurrence. In the late part of the season (September–October), LH anomalies are significant a long time (4–7 days) after the rainfall event in response to persistent soil moisture. In the early part of the rainy season (May–June) the most significant anomalies are found earlier, near the time of rainfall occurrence, possibly as a result of the drier atmosphere and abrupt shift from a dry to a wet surface. Rainfall events are accompanied and followed by

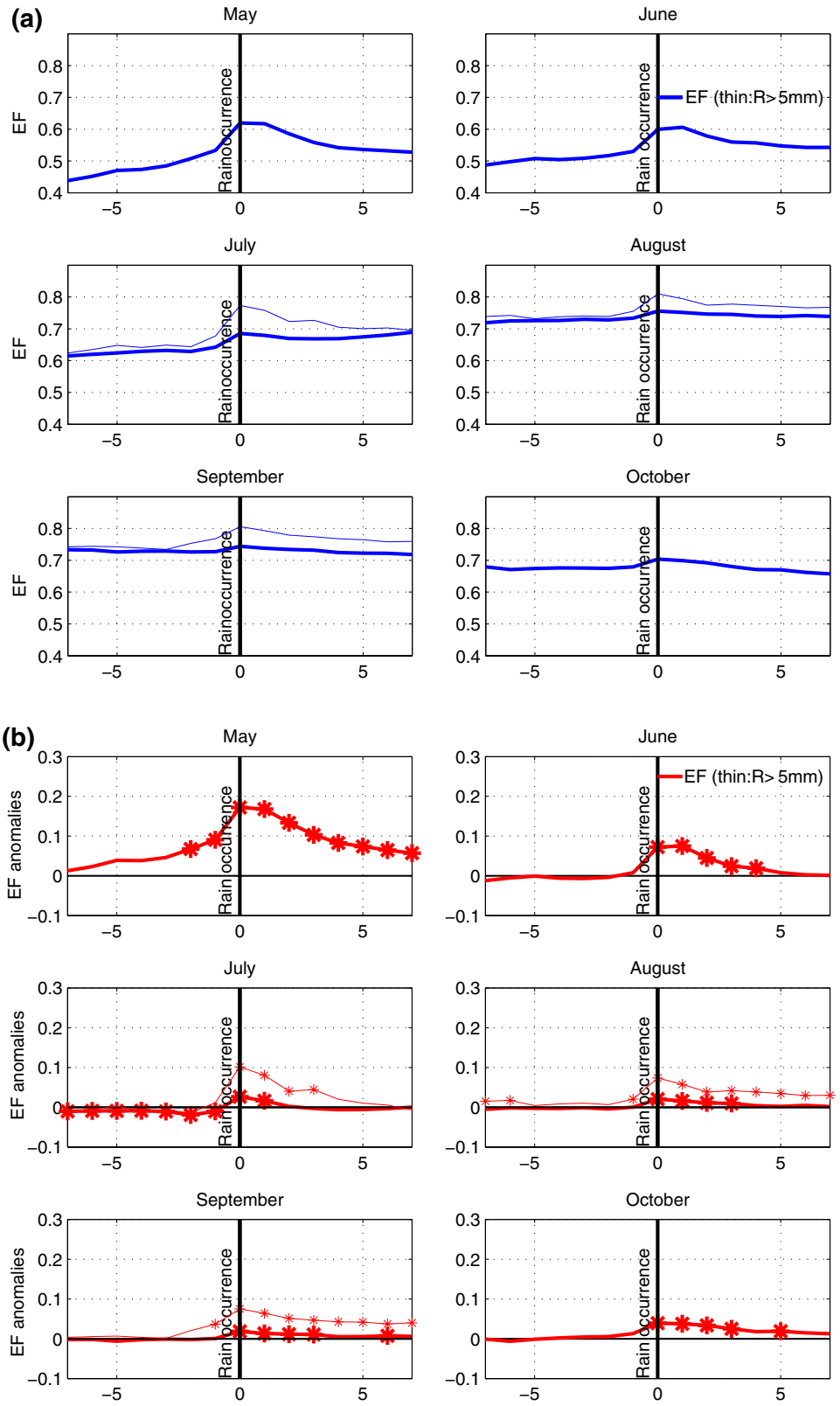

Fig. 9 Composite of evaporative fraction (*EF*) mean (**a**) and anomalies (**b**) over Burkina Faso as a whole (ERA-INTERIM reanalyses, average of all grid-points, period 1983–2008) from 4 days before to 7 days after a rain-day (day 0), from May to October. Rain-days defining the composite sample are days where over 80% of the grid-points received at least 1 mm (*thick lines*) or 5 mm (*thin lines*). *Stars* show significant anomalies (P = 0.99) according to a Student's *t* test

a significant reduction in SH in all months. The magnitude of the rainfall event plays a significant role. For instance, August SH anomalies for rainfall events above 1 mm are at -5 Wm^{-2} on d0, but reach -13 W m^{-2} on the same day for rainfall events above 5 mm. SH anomalies are persistent up to 7 days beyond the heavy (>5 mm) rainfall events in the

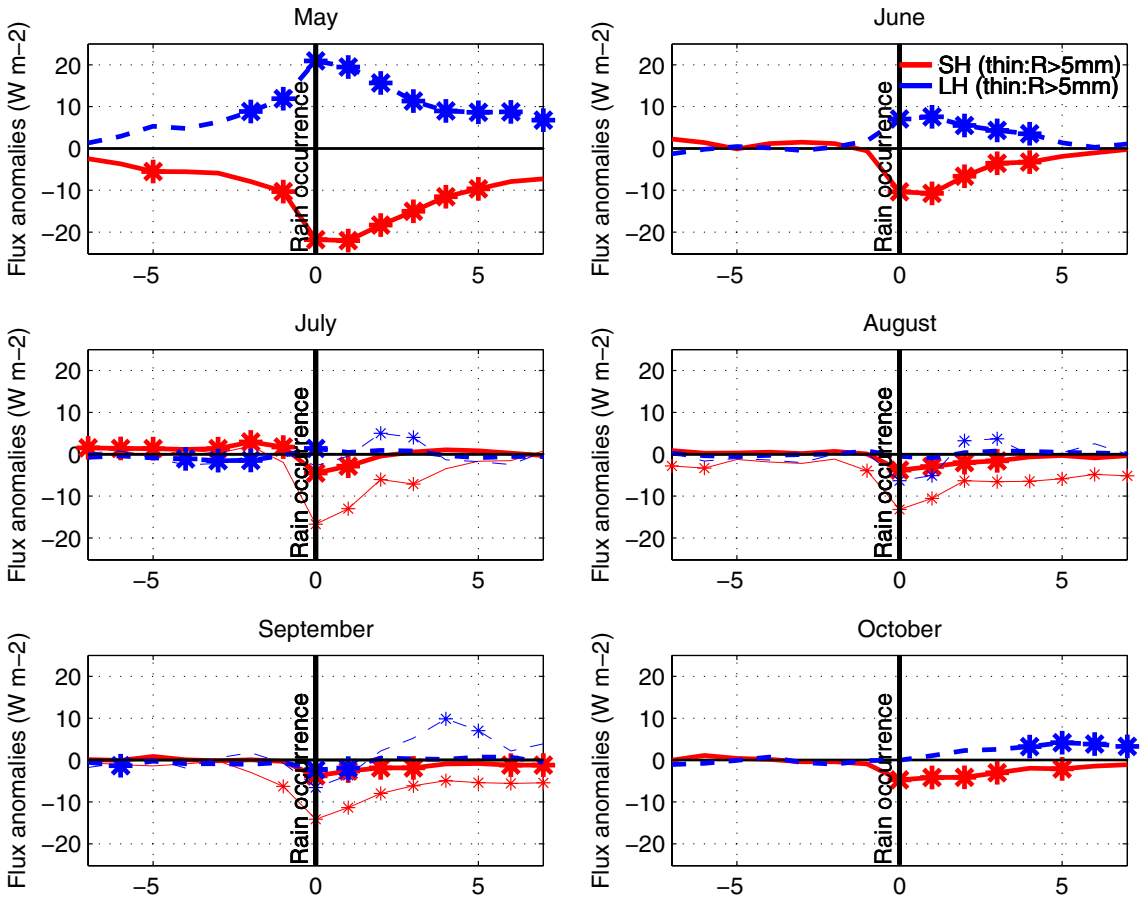

Fig. 10 Composite latent heat (LH) and sensible heat (SH) anomalies over Burkina Faso as a whole (ERA-INTERIM reanalyses, average of all grid-points, period 1983–2008) from 4 days before to 7 days after a rain-day (day 0), from May to October. SH is shown in *red* and *solid lines* and LH in *blue* and *dashed lines*. Rain-days defining the composite sample are days where over 80% of the grid-points received at least 1 mm (*thick lines*) or 5 mm (*thin lines*). Surface turbulent fluxes are counted positive upwards so that positive (negative) anomalies of SH and LH correspond larger (smaller) release of turbulent fluxes into the atmosphere. Stars show significant anomalies (P = 0.99) according to a Student's *t* test

wettest months. Before the wet event, SH values are close to the climatology. The SH negative anomalies during the rainfall event are linked to SWR anomalies (Fig. 6). During rainfall events, less SWR is absorbed by the surface in response to enhanced cloud cover, resulting in a decrease in SH release into the atmosphere. SH can be thus viewed as a consequence of Tx reduction. However, it is a possible cause of Tn reduction. The cooling of the surface during the day results in a reduction of SH during the day and the night, which in turn contributes in cooling Tn.

On the whole, temperature cooling after rainfall events is explained by a reduction in SWR in response to an increase in cloud cover and an increase in surface evaporation in response to surface moistening. Surface evaporation contributes in the persistent cooling several days after the rainfall event. As a result, SH decreases and contributes in Tn cooling. We also analysed the wind patterns associated with rainfall events in ERA-INTERIM (not shown) and found north-easterly anomalies at d0 and d+1, which are not in line with any large-scale advection of cool air (which could have been a possible explanation for Tx and Tn cooling) since in the rainy season the sudano-sahelian belt shows much higher temperatures in the north than in the south.

These conclusions are consistent with Taylor et al. (2005) who found that the modulation of rainfall and cloud over associated with mesoscale convective systems was a key element in the variability of surface fluxes and temperature. They noted that warm and cool regions were well-organized at synoptic scale; with anomalies propagating westwards at a period of about 4–5 days. However, these anomalies could not be directly explained by advection of warm/ cool air, they are mainly determined by the combined effect of surface wetness and incoming solar radiation. Evaporative processes can also affect temperature during a rainfall event through their contribution in

the development of downdrafts and cold pools. In particular, Provod et al. (2015) found that cold pools associated with squall-lines observed at Niamey (Niger) in 2006 were associated with temperature decreases of 2–14 °C. Oueslati et al. (2013) showed that the convective cooling associated with downdrafts weakens the atmospheric boundary layer temperature and associated gradients, which in turn controls the latitudinal position of Intertropical Convergence Zone in the atmospheric general circulation model LMDz. Considering both heavy and total rainfall events, we show that temperature anomalies and associated processes are influenced by precipitation amplitude, which is in contrary to Schwendike et al. (2010) who found that the temperature decline was nearly independent of the amount of precipitation, based on a smaller number of observations. The importance of surface evaporation and shortwave radiation in temperature inter-annual variability was also highlighted in Lenderink et al. (2007). By investigating the surface energy budget in nine different regional climate models, they showed that both fluxes are responsible for model biases in temperature variability.

4 Long-term temperature trends and contribution from rainfall

This section now considers interannual variations of seasonally-averaged Tx, Tn and rainfall. Beyond the description of climatic trends since the late 1950s, the aim is to evaluate whether part of the interannual variations and trends in temperature could be explained by those of rainfall, given the relationship between temperature and rainfall at daily time-scale as documented above.

4.1 Raw temperature and rainfall trends

During the rainy season (May–October), both precipitation and temperature exhibit long-term trends over the 50-year period 1959–2008 (Fig. 11). As an average over Burkina Faso (nine stations), rainfall decreased by about 7% from 1959 to 2008, but the trend is not linear : a strong decrease is found between 1959 and 1984, then a moderate increase is found in the second half of the period. Large interannual fluctuations are superimposed on these trends, in particular in the 1990s. Both the decadal-scale and interannual rainfall variations in Burkina Faso are strongly consistent with

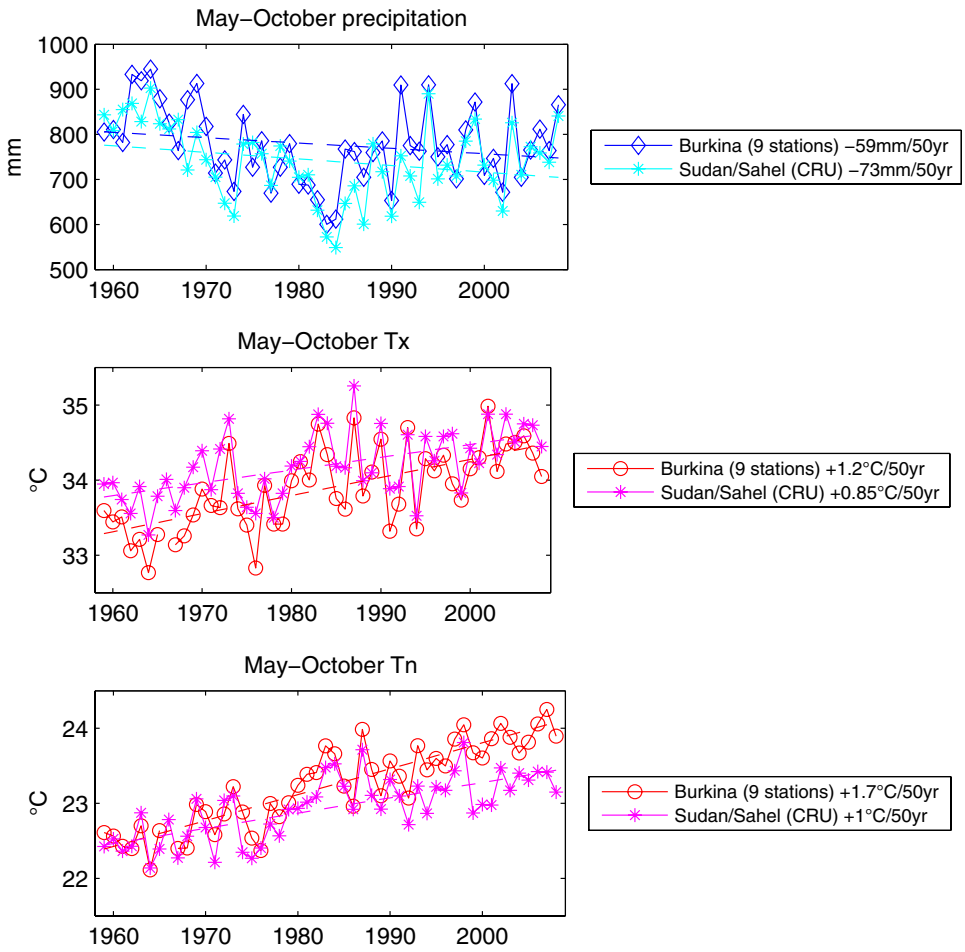

Fig. 11 Mean May–October precipitation and temperature variations over Burkina-Faso (average of nine stations) and the Central Sudan/Sahel (CRU data, 15°W–20°E, 10–15°N), 1959–2008. The legend provides the linear change over the 50-year period

those observed over the central Sudan-Sahel as a whole, as depicted from CRU data (Fig. 11, top panel). They also agree with Nicholson (2005) and Lebel and Ali (2009).

Temperature trends are apparently more linear, both Tx and Tn showing a strong warming since 1959. Over Burkina Faso, May–October Tn increased more than Tx (+1.7 °C as against +1.2 °C). This is a larger increase than over the central Sudan-Sahel as a whole, especially for Tn. Quite large interannual variations are also present, at least for Tx whose extremes ranged from 32.7 °C in 1964 to 35 °C in 2002. These variations are strongly similar to those found in the CRU data for central Sudan-Sahel. The increase is also larger than that found by Moron et al. (2016), but the periods are slightly smaller and their study considers the whole year and a much larger region covering most of tropical North Africa. For July–September, Ringard et al. (2016) found a warming close to +0.3 °C/decade between 1950 and 2012 in the central Sahel, closer to what found for Burkina Faso rainy season. The larger increase in Tn compared to Tx over Burkina Faso is in agreement with observations over the Sahel as a whole over the period 1950–2004 (Zhou et al. 2007).

Given the change found in the precipitation trend around 1984 (strongly decreasing precipitation before this year, increasing precipitation thereafter), slopes of the temperature trends have also been computed separately on the two periods (Table 1). Both Tx and Tn trends are strongly positive in the two periods. However, while Tn rates of increase remained steady, Tx rates declined from +0.49 °C/decade in the period 1959–1983 to +0.28 °C in 1984–2008. Ringard et al. (2016) also found a weakening of the positive trends from the 1980s in the Sahel during July–September, becoming non-significant. This contrasted behavior of temperature before and after the mid-1980s, while the rainfall trends also showed a shift, suggests an association with rainfall.

Correlations between seasonally-averaged values of temperature and rainfall are presented in Table 2, for various periods. Interannual correlations based on detrended time-series are shown between brackets. Strong negative correlations between Tx and rainfall reveal that dry years tend to be abnormally hot, even after removing long-term linear trends. The relationship between Tn and precipitation is less obvious. While in the 1959–1983 sub-period, the raw correlation is highly significant, it is mostly the result of opposite trends (increasing temperature and decreasing rainfall), while after detrending the time-series the correlation becomes insignificant, as in the latter period (1984–2008). These results confirm the strong interactions between precipitation and temperature as discussed above. Linear regressions could be used to analyze the temperature trends after removing the precipitation signal, but at seasonal times-scale it is difficult to separate actual processes from mere covariations. An alternative method is therefore to get back to the daily time-scale, at which the diagnosis on physical processes has been made, to analyze the residual temperature signal.

4.2 Contribution of rainfall to temperature trends

As a first step to extract the rainfall effect on temperature variations, predictive models explaining daily Tx and Tn from concurrent and previous days rainfall were defined (Sect. 2). Table 3 provides, for Tx at Fada N'gourma station as an example, the list of the rainfall predictors retained from the stepwise procedure and the corresponding regression coefficients. As discussed above, both rainfall occurrence and rainfall amounts are used as separate predictors, for attempts to use only one of these group of predictors resulted in lower r-square values. In addition, there is a rationale for considering separately rainfall occurrence and amounts. Rainfall occurrence can be seen as a rough proxy for cloudiness, while rainfall amounts modulates the soil moisture content, thus implying two different driving mechanisms for temperature variations, through the radiative balance and latent heat flux, respectively. For Fada N'gourma, rainfall occurrence on day d0 significantly contributes to a Tx decrease in any month (Table 3). Rainfall occurrence and amounts on previous days also have a significant effect, always negative. Coefficients generally decrease as the lead time increases, but rainfall for days day-3 to day-4 often still contributes significantly to explain temperature variations in most months.

Table 2 Correlation coefficients between seasonally-averaged (May–October) temperature and rainfall variations, for Burkina Faso as a whole (average of nine stations), over the full period and two sub-periods

	1959–2008	1959–1983	1984–2008			
	P	Tx	P	Tx	P	Tx
TX	−0.62** (−0.67)**		−0.75** (−0.61)**		−0.63** (−0.77)**	
TN	−0.33* (−0.35)*	0.84** (0.74)**	−0.68** (−0.32)	0.89** (0.86)**	−0.09 (−0.36)	0.64** (0.61)**

Correlations based on linearly detrended data are shown between brackets. A double (single) star indicates significant values at P = 0.99 (P = 0.95)

Table 3 Regression coefficients from the stepwise models predicting daily Tx (day 0) at Fada N'gourma from daily precipitation occurrence (O) and daily precipitation amounts (A) for day −4 to day 0

	May	June	July	August	September	October
O day0	−10.7	−8.1	−8.7	−11.5	−9.8	−4.4
O day-1	−23.2	−14.6	−11.8	−8.6	−12.0	−10.3
O day-2	−6.8	−5.2	**	−5.1	−5.1	−5.7
O day-3	**	**	−3.6	−3.9	−4.5	**
O day-4	−3.8	**	**	**	−3.5	**
A day-0	**	**	−0.17	**	−0.13	−0.67
A day-1	−0.41	−0.63	−0.23	−0.30	−0.38	−0.96
A day-2	−0.32	−0.32	−0.24	**	−0.18	−0.62
A day-3	−0.41	−0.41	**	**	**	−0.57
A day-4	**	−0.35	−0.20	**	−0.13	−0.62
Multiple corr	0.498	0.475	0.426	0.465	0.561	0.542

Units: tenths of °C per rain day occurrence (O) and tenths of °C per mm (A). Stars indicate that the predictor was not picked in the model at P = 0.95. The last row shows the multiple correlation coefficient

Figure 12 shows daily rainfall variations (bars) and Tx (circled red line) for the month of September in two sample years (1960 and 1995) at Fada N'gourma. The predicted temperature from the multiple regression model for September is plotted (solid blue line). There is a clear Tx decrease accompanying or shortly following most rainfall events. Note that the recovery is sometimes gradual after the rain event. The predicted Tx values replicate quite well the observed Tx variations, although the amplitude of the changes is underestimated, as is typical of regression-based prediction models (Von Storch 1999).

The models are generalized for all stations and months from May to October. Statistics on the rainfall variables included in the 54 models (nine stations × 6 months) as well as the multiple correlation coefficients are shown in Figs. 13 and 14, for Tx and Tn respectively. Multiple correlations are in the range of 0.4 to 0.6 for Tx, with little difference between the months. This indicates that an average

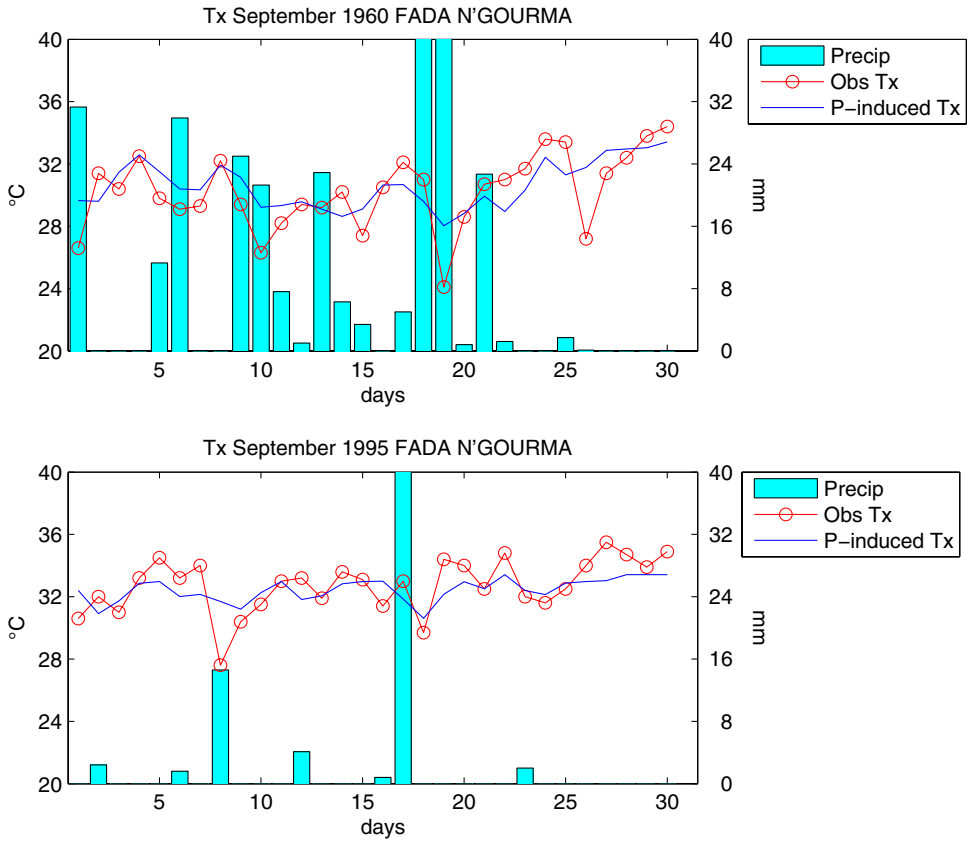

Fig. 12 Daily Tx and precipitation times-series for September of 2 sample years at Fada N'gourma. Observed temperatures: *red line with circles*; temperature as predicted from a multiple regression model based on precipitation occurrence and amount for the whole period 1959–2008: *blue solid line*. See Table 1 for the rainfall predictors retained and the regression coefficients

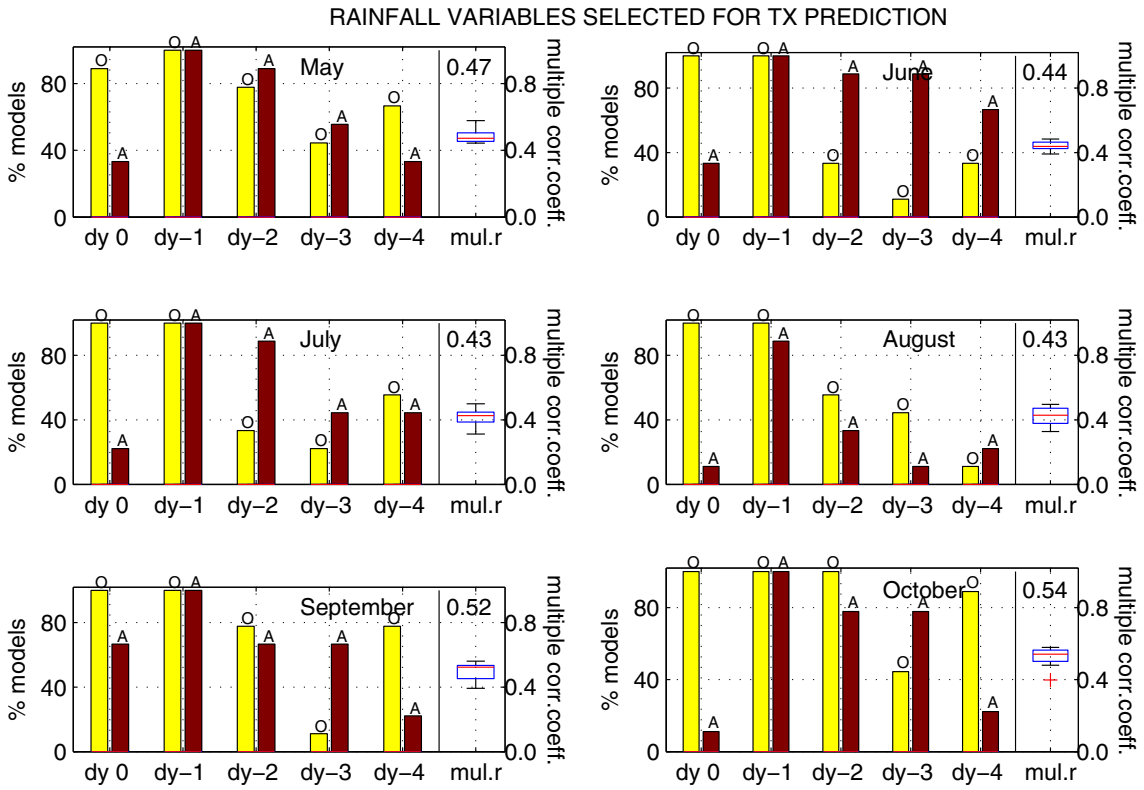

Fig. 13 Summary statistics of multiple linear regression models predicting daily Tx variations on day 0 from rainfall occurrence (O, *yellow bars*) and rainfall amounts (**a**, *brown bars*) from day −4 to day 0, for each month from May to October. *Bars* indicate the number of models (i.e., stations) for which each rainfall variable is retained in the model (P = 0.95). The *boxplot* to the right of each panel shows the distribution of the multiple correlation between Tx and the rainfall predictors retained, across the nine stations of the network (the median correlation value is printed on *top*)

22% of the daily Tx variations are explained by rainfall across Burkina Faso. This is high enough to hypothesize that the rainfall trends significantly contribute to the temperature trends found during the rainy season in Burkina Faso. Figure 13 shows that both rainfall occurrence and amounts explain the daily Tx variations, with a dominant part played by rainfall occurrence on day 0 and a generally greater contribution of rainfall amounts on days day-2 and day-3. As expected the contribution of rainfall decrease with increasing lead time. Models for Tn generally yield higher multiple correlations in the early part of the rainy season (e.g.: May 0.61, June 0.59 as a median value across the nine stations). Rainfall amount is much less often picked up as a predictor than rainfall occurrence, and except at the beginning of the season, rainfall at a long lead time explains little of the Tn variations. This is in accordance with the composite analyses in Sect. 4.

We now shift from the daily to the interannual timescale. Monthly Tx and Tn averages for each year of the period 1959–2008 are computed using both raw data and predicted values from the daily regression models. At this stage, only 6 stations are kept due to too many gaps in the daily temperature time-series to compute monthly averages at three stations. Sample interannual Tx time-series, together with rainfall, are shown in Fig. 15 for Fada N'gourma (July and September). Since 1959, there has been a clear warming trend in both months (+0.34 to 0.35 °C per decade). At the same time, rainfall has been decreasing at a rate of −0.44 to −0.49 mm.day^{-1} per decade. The red lines show Tx estimated from daily rainfall as from the above regression models. Very low rainfall as in July 1967, 1980 and 1984 coincide with high Tx, as predicted from the daily regression models. Wet years (July 1961, 1981 and 1993 for instance) result into abnormally low predicted Tx, in agreement with the observations. The predicted Tx shows a weak positive trend for July (+0.06 °C per decade), much larger in September (+0.18 °C per decade), as a result of the long-term drying trends. There remains quite large differences between predicted and observed Tx in many years. Mean monthly residuals tend to be negative at the beginning of the period, and positive later on. It is these residuals which are next analyzed at all stations combined, to assess temperature trends free from the contribution of rainfall.

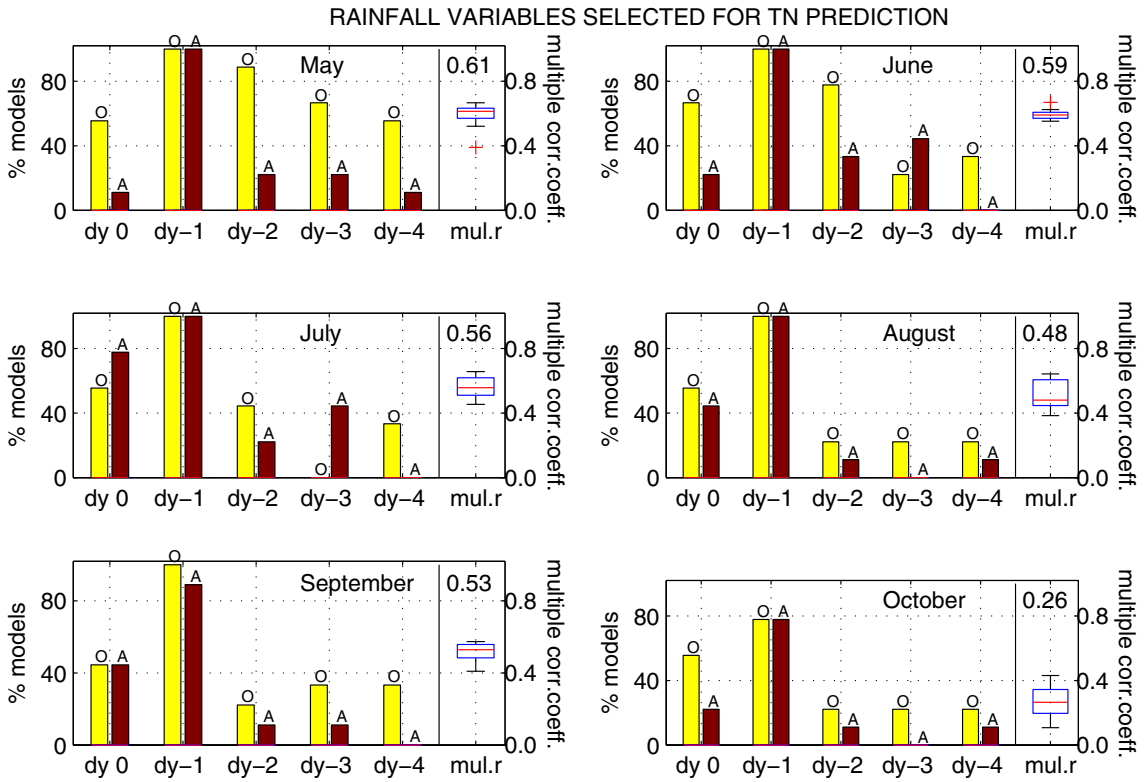

Fig. 14 Same as Fig. 13 but for Tn

The contribution of rainfall variations to linear Tx trends, for the six stations retained for trend analysis and the 6 months (May to October), is shown on Fig. 16. In all the 36 cases, this contribution is that of a warming trend. The most frequent rainfall-induced trend values are comprised between 0.2 and 0.3 °C par decade.

The residual temperature trends (i.e. regression coefficients of Tx and Tn regressed on time), after extraction of the rainfall-induced signal over the period 1959–2008, are shown on Fig. 17, on a monthly basis and as an average over Burkina Faso. The solid red lines stand for trends on raw values, while the dashed red lines are those of the monthly averages residuals, after the contribution of rainfall variations has been removed from the daily temperature data. The black dashed line also shows rainfall trends. A strong warming trend (+0.2 °C to +0.5 °C/decade, i.e. +1 to +2.5 °C during the 50-year period) is found for both Tx and Tn in all months except January and February (for Tx). This warming is strongest near the beginning of the rainy season (April–May), but it is highly significant in the rest of the rainy season as well. As shown above, Tn increased more than Tx, especially in the first part of the year where January–February Tn even warmed significantly contrary to Tx.

The extraction of the contribution from rainfall variations results in smaller warming rates. The rainfall trend has been negative in all months of the rainy season except October. This contributed to a Tx warming exceeding + 0.03 °C per decade from June to September, with a maximum in this latter month (+0.06 °C/decade). Compared to the overall temperature trends, these are small, although significant trends. The highest contribution is in September, where 0.3 °C out of the 1.5 °C total Tx rise during 1959–2008 can be viewed as a result of the drying trend. The rainfall trends contribution to Tn trends is smaller. The drying trend resulted in a warming comprised + 0.015 to +0.036 °C/decade from May to September. This is a very small, almost negligible contribution to the overall Tn increase, which is comprised between +0.32 and +0.49 °C per decade during the rainy season months.

These results therefore show a noticeable effect of rainfall variations on temperature trends, mainly those of Tx, but they do not challenge the strong warming found over Burkina. The fact that the warming rates have been strongly positive in both the early part (1959–1983) and the late part (1984–2008) of the period of study, while in the same time precipitation decreased then slightly increased, is an evidence that the warming of the last 50 years is not entirely related to rainfall variations. However, it is noteworthy that the Tx warming rates have been stronger until 1983 than from 1984 (Table 1). This suggests that in the early part of the record the effect of the drying trend has been to

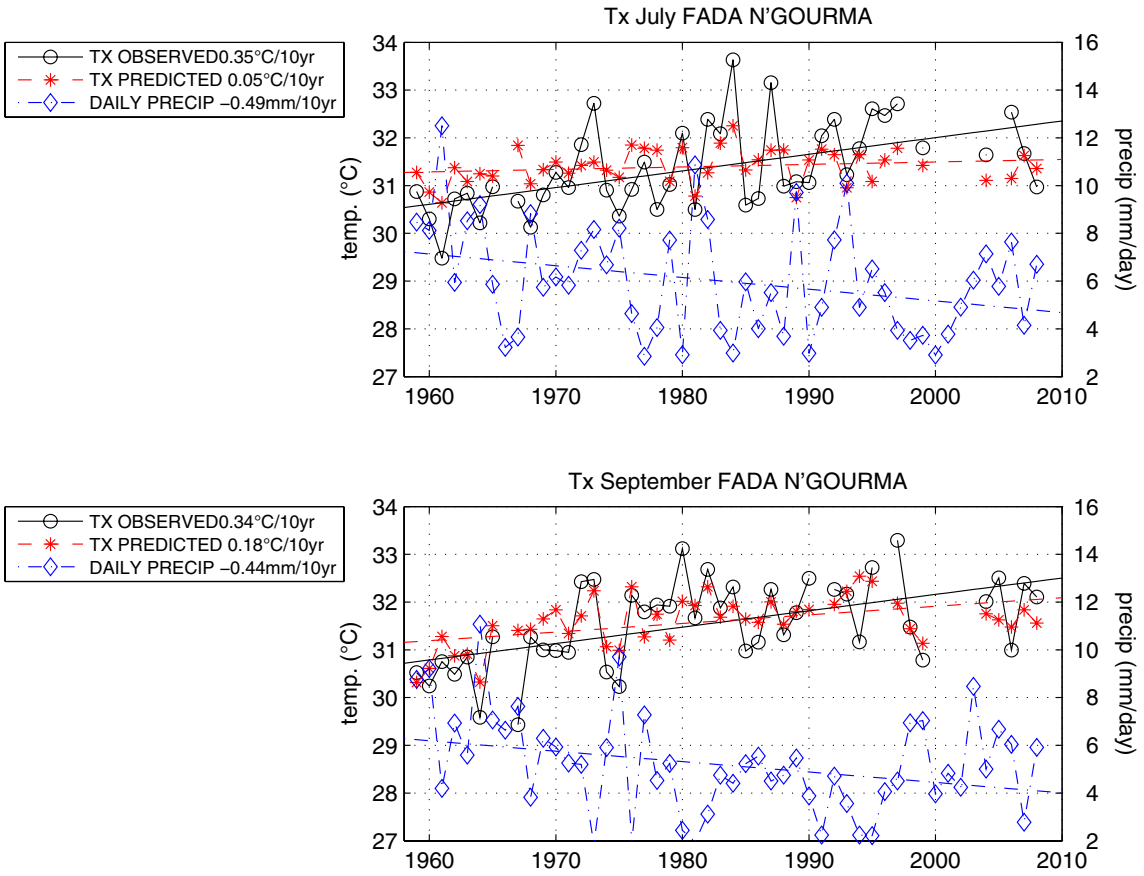

Fig. 15 Interannual variations and trends of maximum temperature (*black solid lines* and *circles*) and rainfall (*blue dashed lines* and *diamonds*) at Fada N'gourma, for July (*top* panel) and September (*bottom panel*). Also shown (*red dashed lines* and *stars*) are the Tx time-series and trends as predicted from the daily precipitation models

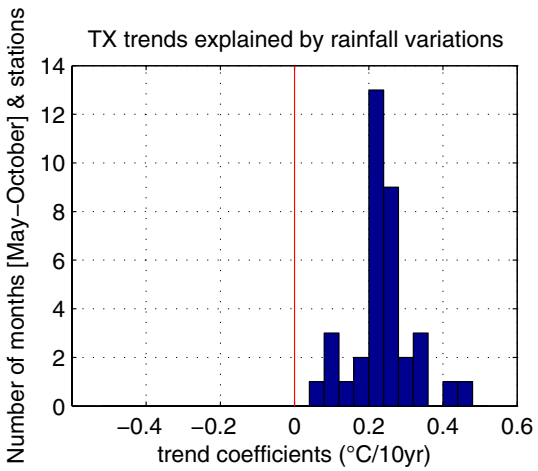

Fig. 16 Histogram of monthly May–October Tx trends (in °C per decade) explained by those of rainfall over the period 1959–2008, for all stations and stations (n = 36). Positive trends mean that the rainfall trend contributed to an increase in Tx

enhance warming. Ringard et al. (2016) actually noted that the Tx trend in July–September has been non linear since 1960 over the Sahel, with a much faster increase before the 1980s than after. The absence of significant Tx and Tn trends since the 1980s in the Sahel is likely related to the wetting trend, as found in Burkina Faso. Also in line with our study, Zhou et al. (2007) demonstrated that the DTR variations in the Sahel region are inversely related to those of rainfall and clouds, but long-term changes in rainfall and cloud cover cannot fully account for the DTR trend.

5 Conclusion

The analysis of 50 years (1959–2008) of observed temperature (Tx and Tn) and rainfall variations in the central Sudano-Sahelian belt revealed strong interactions between these variables. At daily times-scale, both Tx and Tn show a marked decrease as a response to rainfall occurrence, with the largest departure from normal 1 day after the rainfall event (from −0.5 to −2.5 °C depending on the month).

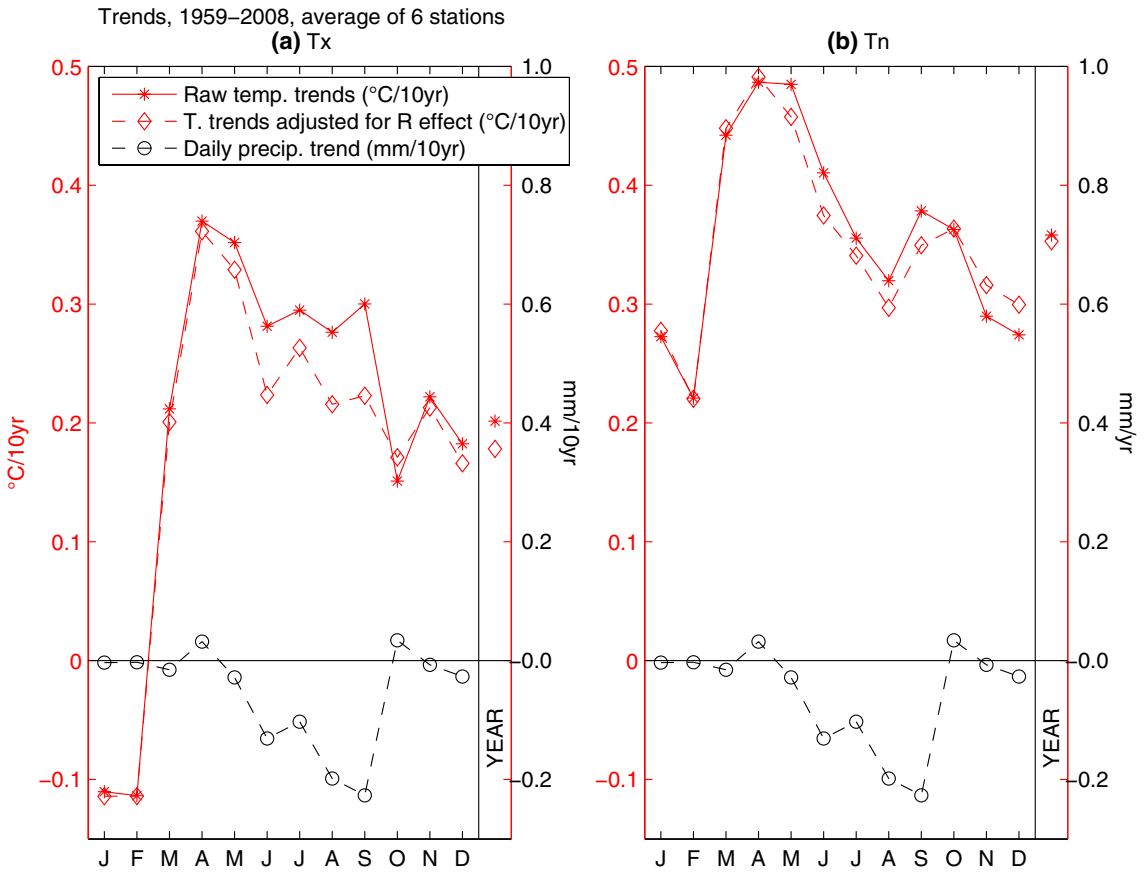

Fig. 17 Monthly and yearly trends of maximum temperature (*left panel*) and minimum temperature (*right panel*) as an average over Burkina-Faso, 1959–2008 (°C.decade^{-1}). *Solid line with stars*: raw temperature data; *dashed line with diamonds*: temperature trend adjusted from precipitation effect. The *bottom dashed lines with circles* show the precipitation trends (mm.decade^{-1})

The cooling is slightly stronger when heavy rainfall events (>15 mm) are considered. The temperature anomalies weaken in the following days, but a significant cooling can still be found several days after the rainfall event, mainly in Tx and at the beginning and end of the rainy season. The amplitude of the temperature response is also larger in the early and late phases of the rainy season. These relationships between daily temperature variations and precipitation events markedly differ from those found in other climatic environments like most of Canada (Isaac and Stuart 1992) where, across a wide range of situations, many areas show positive associations (more precipitation related to warmer weather). Contrasted patterns were also found in the Eastern Horn of Africa (Camberlin 2016), where highlands stations often display lower Tx but higher Tn associated with rainfall events, whereas lowland, semi-arid locations have temperature anomaly patterns close to those found in Burkina Faso.

Reanalysis data (ERA-INTERIM) reproduce reasonably well the temperature response to rainfall occurrence. A slight phase shift, seen in the maximum cooling being as strong on day 0 than on day+1, can be explained by some differences in the reference 24-h period between the observation and the reanalysis data. The reanalysis data, supplemented by CERES satellite observations, indicate that the initial Tx drop is accounted for by reduced incoming solar radiation and increased surface evaporation. A smaller increase in net longwave radiation, resulting from enhanced water vapor anomalies rather than from the cloud cover, does not compensate the lower incoming shortwave radiation. These changes in radiative fluxes are short lasting. Changes in turbulent fluxes are more durable. An increased latent heat flux from the surface to the atmosphere, as a result of the moistened land surface, follows the rainfall event. The peak in the latent flux anomaly occurs gradually later as the season advances (from 2 days to 5 days after the rain event, from July to October) following the gradual increase of net shortwave radiation 2 days after the rainfall event. It is suggested that evaporation is controlled not only by moisture availability but also by net radiative energy as suggested by previous studies (e.g. Koster et al. 2004). Shortwave radiation anomalies are larger at the end of the

wet season favoring more surface evaporation. A decrease in sensible heat flux, significant from the rainfall event up to 3–7 days later, is linked to the latent heat increase and can be viewed as a response of temperature changes themselves.

The kind and scale of the data used at this stage are not accurate enough to have a thorough understanding of the mechanisms of the temperature-rainfall interactions, but they are useful in showing theimportant role of reduced solar radiation (in consistency with Guichard et al. 2009, and Mamadou et al. 2014), which reduces Tx, the daytime heat storage and the subsequent sensible heat flux, resulting in a later negative Tn anomaly. This is not compensated by the increased net longwave radiation. The increased latent flux resulting from evaporation is also contributing to the negative temperature anomaly, becoming dominant a few days after the rainfall event and in the second part of the rainy season.

Relationships between temperature and precipitation were next examined at interannual time-scales. Strong negative correlations are found between Tx and precipitation, even after detrending. For Tn the relationship is weaker and not significant. At global scale, negative correlations between seasonal mean temperatures and precipitation actually dominate, at least over land and in summer or in the main rainy season in the tropics (Adler et al. 2008; Berg et al. 2015). Since the Sahelian climate has undergone strong decadal-scale and long-term variations since the mid-twentieth century, and given the significant temperature-precipitation relationships, the contribution of rainfall trends to those of temperature has been analysed. Over Burkina Faso, climate trends are broadly similar to those depicted for the rest of the sudano-sahelian belt, with a strong drying-up between 1959 and 1984 followed by a weaker precipitation increase, while both Tn and Tx increased (except in boreal winter), in agreement with Ringard et al. (2016) and Moron et al. (2016).. However, the rate of Tx increase has been much slower (and even non-significant) in the second part of the period, during which rainfall recovered. We demonstrated that taking into account the precipitation trends in Burkina Faso helps in understanding the particulars of wet season temperature trends in the last decades. The strong Tx warming trend found in the first half of the period, as in the central Sahel as a whole (Ringard et al. 2016), is partly the result of the drought conditions found in the 1970s and early 1980s. Reciprocally, the absence of statistically significant trends since the 1980s (Ringard et al. 2016) can be ascribed to the partial return to wetter conditions, which resulted in almost canceling out the long-term warming likely associated with enhanced GHG. In the longer-term, and based on multivariate regression models relating daily temperature variations to rainfall, the precipitation trend between 1959 and 2008 accounted for a rainy season Tx increase of 0.15 to 0.3 °C, out of a total Tx increase of 1.3 to 1.5 °C. Tn changes were only marginally influenced by those of rainfall.

The noticeable effect of rainfall variations on temperature trends have strong implications on future changes in response to global warming. Cattiaux et al. (2013) studied the temperature inter-model spread in Europe and highlighted the important roles of local radiative effects and SST changes. As already highlighted in the mid-latitudes (e.g. Douville et al. 2016), precipitation projections will indeed tend to amplify or dampen temperature warming in the Sudano-Sahelian zone depending on the sign of rainfall change. Precipitation projections still exhibit large inter-model uncertainties in many regions, including the Sahel (e.g. Oueslati et al. 2016), resulting in discrepancies in future temperature changes. However, despite these uncertainties it is possible to detect in the XXI century projections a significant decrease of rainfall amounts in the Western Sahel, and an increase over the Central and Eastern Sahel including Burkina Faso (Monerie et al. 2013). This suggests that the temperature trends associated to the global warming could be different in the various parts of the Sahel.

Large efforts are thus needed to investigate the temperature-precipitation coupling in the recent and future climate by examining this relationship in regional and global simulations, as well as associated physical processes. Two types of processes are identified as drivers of the precipitation-temperature interaction: the shortwave cloud radiative effect and soil moisture control on evaporation. The role of shortwave cloud radiative effect could be addressed by using COOKIE (Clouds On/Off Klimate Intercomparison Experiment) numerical experiments in which clouds are made transparent to radiation (Stevens et al. 2012). The soil moisture-temperature coupling could be investigated using regional and global simulations of recent and future climatic conditions with varying land–atmosphere interactions (e.g. Seneviratne et al. 2006; Berg et al. 2015). These experiments are planned in the Land Surface, Snow and Soil Moisture Model Intercomparison Project (LS3MIP; Van Den Hurk et al. 2016) as part of the sixth phase of the Coupled Model Intercomparison Project (CMIP6). Advancing our understanding of these processes is crucial to gain confidence on climate projections, anticipate future changes and develop adequate adaptation strategies.

References

Adler RF, Gu G, Wang JJ, Huffman GJ, Curtis S, Bolvin D (2008) Relationships between global precipitation and surface temperature on interannual and longer timescales (1979–2006). J Geophys Res 113:D22104. doi:10.1029/2008JD010536

Berg A, Lintner BR, Findell K, Seneviratne SI, van den Hurk B, Ducharne A, Gentine P (2015) Interannual coupling between summertime surface temperature and precipitation over land: processes and implications for climate change. J Clim 28(3):1308–1328. doi:10.1175/JCLI-D-14-00324.1

Betts AK, Köhler M, Zhang Y (2009) Comparison of river basin hydrometeorology in ERA-Interim and ERA-40 reanalyses with observations. J Geophys Res Atmos 114(D2)

Camberlin P (2016) Temperature trends and variability in the Greater Horn of Africa: interactions with precipitation. Clim Dyn doi:10.1007/s00382-016-3088-5

Cattiaux J, Douville H, Peings Y (2013) European temperatures in CMIP5: origins of present-day biases and future uncertainties. Clim Dyn 41(11–12):2889–2907

Collins JM (2011) Temperature variability over Africa. J Clim 24(14):3649–3666

Dai A, Trenberth KE, Karl TR (1999) Effects of clouds, soil moisture, precipitation, and water vapor on diurnal temperature range. J Clim 12(2451):2473

De Longueville F, Hountondji YC, Kindo I, Gemenne F, Ozer P (2016) Long-term analysis of rainfall and temperature data in Burkina Faso (1950–2013). Int J Clim

Dee DP et al. (2011) The ERA-interim reanalysis: configuration and performance of the data assimilation system. Quart J Roy Meteor Soc 137:553–597

Déry SJ, Wood EF (2005) Observed twentieth century land surface air temperature and precipitation covariability. Geophys Res Lett 32(21):L21414. doi:10.1029/2005GL024234

Dong B, Sutton RT, Shaffrey L (2016) Understanding the rapid summer warming and changes in temperature extremes since the mid-1990s over Western Europe. Clim Dyn. doi:10.1007/s00382-016-3158-8

Douville H, Colin J, Krug E, Cattiaux J, Thao S (2016) Midlatitude daily summer temperatures reshaped by soil moisture under climate change. Geophys Res Lett

Fischer EM, Sereviratne SI, Vidale PL, Luthi D, Schaer C (2007a) Soil moisture–atmosphere interactions during the 2003 European summer heat wave. J Clim 20:5081–5099

Fischer EM, Sereviratne SI, Luthi D, Schar C (2007b) Contribution of land–atmosphere coupling to recent European summer heat waves. Geophys Res Lett 34:L06707

Fontaine B, Janicot S, Monerie P-A (2013) Recent changes in air temperature, heat waves occurrences and atmospheric circulation in Northern Africa. J Geophys Res Atmos 118:536–552

Guichard F, Kergoat L, Mougin E, Timouk F, Baup F, Hiernaux P, Lavenu F (2009) Surface thermodynamics and radiative budget in the Sahelian Gourma: seasonal and diurnal cycles. J Hydrol 375(1):161–177

Guichard F, Kergoat L, Taylor CM, Cappelaere B, Chong M, Couvreux F, Lothon M (2012) Interactions entre surface et convection au Sahel. La Météorol (1):25–32

Harris I, Jones PD, Osborn TJ, Lister DH (2014) Updated high-resolution grids of monthly climatic observations—the CRU TS3.10 dataset. Int J Climatol 34:623–642. doi:10.1002/joc.3711

Isaac GA, Stuart RA (1992) Temperature-precipitation relationships for Canadian stations. J Clim 5:822–830

Koster RD, Dirmeyer PA, Guo Z, Bonan G, Chan E, Cox P, Liu P (2004) Regions of strong coupling between soil moisture and precipitation. Science 305(5687):1138–1140

Lebel T, Ali A (2009) Recent trends in the Central and Western Sahel rainfall regime (1990–2007). J Hydrol 375(1):52–64

Lenderink G, van Ulden A, van den Hurk B, van Meijgaard E (2007) Summertime inter-annual temperature variability in an ensemble of regional model simulations: analysis of the surface energy budget. Clim Chang 81:233–247

Lodoun T, Giannini A, Traoré PS, Somé L, Sanon M, Vaksmann M, Rasolodimby JM (2013) Changes in seasonal descriptors of precipitation in Burkina Faso associated with late 20th century drought and recovery in West Africa. Environ Dev 5:96–108

Lohou F, Kergoat L, Guichard F, Boone A, Cappelaere B, Cohard JM, Ramier D (2014) Surface response to rain events throughout the West African monsoon. Atmos Chem Phys 14(8):3883–3898

Lorenz R, Argüeso D, Donat M, Pitman A, van den Hurk B, Berg A, Lawrence D, Cheruy F, Ducharne A, Hagemann S, Meier A, Milly C, Seneviratne S (2016) Influence of land-atmosphere feedbacks on temperature and precipitation extremes in the GLACE-CMIP5 ensemble. JGR-atmos 121:607–623

Lott N, Vose R, Del Greco SA, Ross T, Worley S, Comeaux J (2008) The integrated surface database: partnerships and progress. In Proceedings of 88th AMS Annual Meeting—American Meteorological Society, New Orleans, 20–24 January 2008, 1–3

Mamadou O, Cohard JM, Galle S, Awanou CN, Diedhiou A, Kounouhewa B, Peugeot C (2014) Energy fluxes and surface characteristics over a cultivated area in Benin: daily and seasonal dynamics. Hydrol Earth Syst Sci 18(3):893–914

Menne MJ, Durre I, Vose RS, Gleason BE, Houston TG (2012) An overview of the global historical climatology network daily database. J Atmos Ocean Tech 29:897–910

Monerie P-A, Roucou P, Fontaine B (2013) Mid-century effects of climate change on African monsoon dynamics using the A1B emission scenario. Int J Climatol 33(4):881–896. doi:10.1002/joc.3476

Moron V, Oueslati B, Pohl B, Rome S, Janicot S (2016) Trends of mean temperatures and warm extremes in Northern Tropical Africa (1961–2014). J Geophys Res Atmos 121:5298–5319

Nicholson S (2005) On the question of the "recovery" of the rains in the West African Sahel. J Arid Environ 63(3):615–641

Nikulin G, Jones C, Giorgi F, Asrar G, Büchner M, Cerezo-Mota R, van Meijgaard E (2012) Precipitation climatology in an ensemble of CORDEX-Africa regional climate simulations. J Clim 25(18):6057–6078

Oueslati B, Bellon G (2013) Tropical precipitation regimes and mechanisms of regime transitions: contrasting two aquaplanet general circulation models. Clim Dyn 40:2345–2358

Oueslati B, Bony S, Risi C, Dufresne JL (2016) Interpreting the inter-model spread in regional precipitation projections in the tropics: role of surface evaporation and cloud radiative effects. Clim Dyn 47:2801–2815

Oueslati B, Pohl B, Moron V, Rome S, Janicot S (2017) Characterisation of heat waves in the Sahel and associated physical mechanisms. J Clim. doi:10.1175/JCLI-D-16-0432.1

Pan Z, Arritt RW, Takle ES, Gutowski WJ, Anderson CJ, Segal M (2004) Altered hydrologic feedback in a warming climate introduces a "warming hole". Geophys Res Lett 31(17)

Portmann RW, Solomon S, Hegerl GC (2009) Spatial and seasonal patterns in climate change, temperatures, and precipitation across the United States. Proc Natl Acad Sci USA 106(18):7324–7329

Provod M, Marsham JH, Parker DJ, Birch CE (2015) A characterization of cold pools in the West African Sahel. Mon Wea Rev 144(5):1923–1934

Ringard J, Dieppois B, Rome S, Diedhiou A, Pellarin T, Konaré A, Sanda IS (2016) The intensification of thermal extremes in west Africa. Global Planet Change 139:66–77

Roca R, Chambon P, Jobard I, Kirstetter PE, Gosset M, Bergès JC (2010) Comparing satellite and surface rainfall products over West Africa at meteorologically relevant scales during the AMMA campaign using error estimates. J Appl Meteorol Climatol 49(4):715–731

Rohde R, Muller R, Jacobsen R, Perlmutter S, Mosher S (2013) Berkeley earth temperature averaging process. Geoinform Geostat. doi:10.4172/2327-4581.1000103

Rutan DA, Kato S, Doelling DR, Rose FG, Nguyen LT, Caldwell TE, Loeb NG (2015) CERES synoptic product: methodology and validation of surface radiant flux. J Atmos Ocean Technol 32(6):1121–1143

Schwendike J, Kalthoff N, Kohler M (2010) The impact of mesoscale convective systems on the surface and boundary-layer structure in West Africa: case-studies from the AMMA campaign 2006. Quart J Roy Meteor Soc 136(648):566–582

Seneviratne SI, Luthi D, Litschi M, Schar C (2006) Land–atmosphere coupling and climate change in Europe. Nature 443:205–209

Seneviratne S, Wilhelm M, Stanelle T, van den Hurk B, Hagemann S, Berg A, Cheruy F, Higgins M, Meier A, Brovkin V, Claussen M, Dufresne J-L, Findell K, Lawrence D, Malyshev S, Smith B (2013) Impact of soil moisture-climate feedbacks on CMIP5 projections: First results from the GLACE-CMIP5 experiment. Geophys Res Lett 40:5212–5217

Stevens B, Bony S, Webb M (2012) Clouds on-off klimate intercomparison experiment (COOKIE). http://www.euclipse.eu/wp4/wp4.html. Accessed 31 March 2017

Sun Y, Solomon S, Dai A, Portmann RW (2006) How often does it rain?. J Clim 19:916–934

Tang Q, Leng G (2012) Damped summer warming accompanied with cloud cover increase over Eurasia from 1982 to 2009. Environ Res Lett 7(1):014004. doi:10.1088/1748-9326/7/1/014004

Tang Q, Leng G (2013) Changes in cloud cover, precipitation, and summer temperature in North America from 1982 to 2009. J Clim 26(5):1733–1744

Taylor CM, Parker DJ, Lloyd CR, Thorncroft CD (2005) Observations of synoptic-scale land surface variability and its coupling with the atmosphere. Quart J Roy Met Soc 131(607):913–937

Taylor CM, Gounou A, Guichard F, Harris PP, Ellis RJ, Couvreux F, De Kauwe M (2011) Frequency of Sahelian storm initiation enhanced over mesoscale soil-moisture patterns. Nat Geosci 4(7):430–433

Trenberth KE, Shea DJ (2005) Relationships between precipitation and surface temperature. Geophys Res Lett 32:L14703. doi:10.1029/2005GL022760

Van Den Hurk B, Kim H, Krinner G, Seneviratne SI, Derksen C, Sheffield J (2016) LS3MIP (v1.0) contribution to CMIP6: the land surface, snow and soil moisture model intercomparison project: aims, setup and expected outcome. Geosci Model Dev 9(8):2809–2832

Von Storch H (1999) On the use of ''inflation'' in statistical downscaling. J of Clim 12:3505–3506

World Meteorological Organization (2009) Handbook on CLIMAT and CLIMAT TEMP Reporting, WMO/TD-No. 1188, Geneva

Yu S, Alapaty K, Mathur R, Pleim J, Zhang Y, Nolte C, Nagashima T (2014) Attribution of the United States "warming hole": aerosol indirect effect and precipitable water vapor. Sci Rep 4:6929

Zhou L, Dickinson RE, Tian Y, Vose RS, Dai Y (2007) Impact of vegetation removal and soil aridation on diurnal temperature range in a semiarid region: application to the Sahel. Proc Nat Acad Sci 104(46):17937–17942

Zhou L, Chen H, Dai Y (2015) Stronger warming amplification over drier ecoregions observed since 1979. Envir Res Lett 10(6):064012